Biophysical Journal Volume 65 July 1993 270–288

Theoretical Reconstruction of Myotonia and Paralysis Caused by Incomplete Inactivation of Sodium Channels

Stephen C. Cannon,*‡ Robert H. Brown, Jr.,*§ and David P. Corey*‡¶

*Department of Neurology, Massachusetts General Hospital, Boston, Massachusetts 02114 USA; ‡Howard Hughes Medical Institute, Massachusetts General Hospital, Boston, Massachusetts 02114; §Day Neuromuscular Research Laboratory, Charlestown Neuroscience Center, Charlestown, Massachusetts 02129, and ¶Program in Neuroscience, Harvard Medical School, Boston, Massachusetts 02115 USA

ABSTRACT Muscle fibers from individuals with hyperkalemic periodic paralysis generate repetitive trains of action potentials (myotonia) or large depolarizations and block of spike production (paralysis) when the extracellular K^+ is elevated. These pathologic features are thought to arise from mutations of the sodium channel α subunit which cause a partial loss of inactivation (steady-state $P_{open} \approx 0.02$, compared to < 0.001 in normal channels). We present a model that provides a possible mechanism for how this small persistent sodium current leads to repetitive firing, why the integrity of the T-tubule system is required to produce myotonia, and why paralysis will occur when a slightly larger proportion of channels fails to inactivate.

The model consists of a two-compartment system to simulate the surface and T-tubule membranes. When the steady-state sodium channel open probability exceeds 0.0075, trains of repetitive discharges occur in response to constant current injection. At the end of the current injection, the membrane potential may either return to the normal resting value, continue to discharge repetitive spikes, or settle to a new depolarized equilibrium potential. This after-response depends on both the proportion of noninactivating sodium channels and the magnitude of the activity-driven K^+ accumulation in the T-tubular space. A reduced form of model is presented in which a two-dimensional phase-plane analysis shows graphically how this diversity of after-responses arises as extracellular $[K^+]$ and the proportion of noninactivating sodium channels are varied.

INTRODUCTION

Several laboratories have recently proposed that many inherited forms of myotonia and periodic paralysis may be caused by a failure of the voltage-gated sodium channel to inactivate normally (reviewed in Ref. 1). With the three-electrode voltage clamp, Lehmann-Horn, Rüdel, and colleagues discovered a noninactivating, tetrodotoxin (TT)-sensitive, inward current in fibers biopsied from patients with hyperkalemic periodic paralysis (HPP) (2–4) and paramyotonia congenita (PC) (5) that was absent in normal muscle. We showed that, in the presence of 10 mM extracellular K^+, sodium channels from HPP muscle entered a noninactivating mode of gating in 5–10% of trials as evidenced by prolonged open times and persistent reopenings (6). Both HPP and PC are inherited in an autosomal dominant manner with high penetrance. All families studied thus far with HPP and PC have demonstrated tight genetic linkage with no recombinations to SCN4A, the genetic locus of the α subunit of the adult isoform of the skeletal muscle sodium channel on chromosome 17q (7–9). Several different point mutations have been identified in SCN4A from families with HPP (10, 11) and PC (12). When the HPP mutations are introduced into the sodium channel cDNA isolated from rat skeletal muscle, the expressed channels fail to inactivate completely (13). Incomplete inactivation of sodium channels has also been recorded in cell-attached patches of muscle biopsied from patients with myotonic dystrophy (14), generalized recessive myotonia (15), and the Schwartz-Jampel Syndrome (16). For these latter three disorders, however, genetic analysis has not yet established linkage to nor identified a mutation in SCN4A.

If a disruption of sodium channel inactivation is to be accepted as a possible cause of some forms of myotonia and periodic paralysis, then it is crucial to establish that the identified functional defect in channel gating is sufficient to cause the phenotype. In a previous study, we created an in vitro model of the sodium channel defect by applying a polypeptide toxin from *Anemonia sulcata* (ATX II) to a fast twitch muscle of the rat hindleg (17). Those experiments demonstrated that self-sustained trains of action potentials and myotonic twitch responses develop when the muscle is bathed in 10 μm ATX II. At that concentration of toxin, sodium currents in the sarcolemma had a noninactivating open probability of 0.015–0.02 at −10 mV. This degree of inactivation failure is at the lower end of the range that was recorded in myotubes cultured from a patient with HPP (6). We presume that paralysis would have been produced if we could have disrupted inactivation for a larger proportion of sodium channels—an extrapolation that can easily be achieved in a computational model.

The aim of the present study is to investigate how an alteration in sodium channel gating influences the electrical excitability of the entire muscle fiber. Previous simulations with the Hodgkin-Huxley equations for the squid axon at 6°C have shown that noninactivating sodium channels can cause a new resting state at depolarized potentials and can lead to repetitive discharges if the peak K^+ conductance is lowered or if deactivation of the sodium current is slowed (18, 19). Our model uses parameters for conductances measured in

Received for publication 16 December 1992 and in final form 24 March 1993.

Address reprint requests to Stephen C. Cannon, Wellman 414, Massachusetts General Hospital, Boston, MA 02114.

0006-3495/93/07/270/19 $2.00

mammalian muscle at room temperature, and more importantly, incorporates a T-tubule compartment which significantly increases the membrane impedance in comparison to nerve and which forms a diffusion-limited space for the activity-driven accumulation of K^+. The model is complete enough to simulate the main features of normal, myotonic, and paralytic muscle, and yet simplified enough to allow intuitive insight as to how incomplete inactivation of the sodium conductance alters the overall behavior. Membrane potential transients recorded from rat muscle that was exposed to anemone toxin are presented for comparison to the model responses.

THEORY

A two-compartment model for muscle

In the present model, the internal resistivity of the muscle fiber is assumed to be negligible. This assumption implies that the fiber is space-clamped such that all points of the sacrolemmal membrane are at the same potential and action potentials are nonpropagated in space. We think this approximation is a reasonable starting point since, in a previous model of fibers with a low chloride conductance by Adrian and Marshall (20), the tendency to produce myotonic versus normal action potentials did not depend strongly on propagation parameters (internal resistivity or fiber diameter). Furthermore, this approximation simplifies the membrane equations such that an intuitive understanding may be retained, and it reduces the computational task tremendously.

A common feature of myotonia arising from distinctly different channel defects, either incomplete inactivation of the sodium conductance in ATX II-treated fibers (17) or a low chloride conductance in the myotonic goat (21), is a dependence on the integrity of the T-tubule system. Thus a minimally sufficient model must incorporate both surface and T-tubular membrane compartments. In the current theory, we will assume that the T-tubular membrane is space-clamped radially so that the entire T-tubule attached to a unit area of surface membrane can be modeled as a single compartment.

The total current passing between the sarcoplasm and the extracellular fluid/unit area of surface membrane, I_m (mA/cm^2), is a combination of the capacitive, ionic and T-tubular components as shown in Fig. 1.

$$I_m = I_c + I_{ionic} + I_t \tag{1}$$

The T-tubule and extracellular fluid spaces are separated by an access resistance at the vestibule of the tubule, R_a (150 ohm-cm^2 (22)), so that I_t may be computed as:

$$I_t = \frac{V - V_t}{R_a} \tag{2}$$

where V is the potential across the surface membrane, V_t is the potential difference across the T-tubular membrane. Notice that I_t is the total current leaving the T-tubular system/unit area of *surface* membrane. Substituting Eq. 2 into Eq. 1 and expressing I_c in terms of the capacitance/unit area of surface membrane, C_m (1 μF/cm^2), yields equation (3) as follows.

$$I_m = C_m \frac{dV}{dt} + I_{ionic} + \frac{V - V_t}{R_a} \tag{3}$$

The analogous current balance may be written for the T-tubular membrane. The specific capacitance/unit area of membrane, C_m, is assumed to be identical for both the surface and T-tubule membranes. Ionic currents through voltage-gated channels are included in the T-tubule membrane. Equation 4 describes the current flowing across the total area of T-tubule membrane attached to 1 cm^2 of surface membrane.

$$\frac{V - V_t}{R_a} = \gamma C_m \frac{dV_t}{dt} + \gamma \hat{I}_{ionic} \tag{4}$$

The carat is to explicitly denote current density/unit area of T-tubular membrane for the ionic current. γ is the ratio of the T-tubular membrane area/unit area of surface membrane and equals 4.8 for a fiber with a radius of 40 μm (Adrian et al. (23), based on measurements by Peachy (24)).

The ionic currents consist of a leak current with a constant conductance, a delayed rectifier K^+ current and a regenerative Na^+ current. The latter two are approximated by the Hodgkin-Huxley equations which empirically describe the time and voltage dependence of the open probability for each channel type. The voltage-gated ion channels in the T-tubule are assumed to have the same kinetics and conductances as those of the surface membrane. The density of ion channels, however, is not necessarily the same for the two membranes. The open-channel I-V relationship for all channels is assumed to be ohmic. The ionic currents for the surface

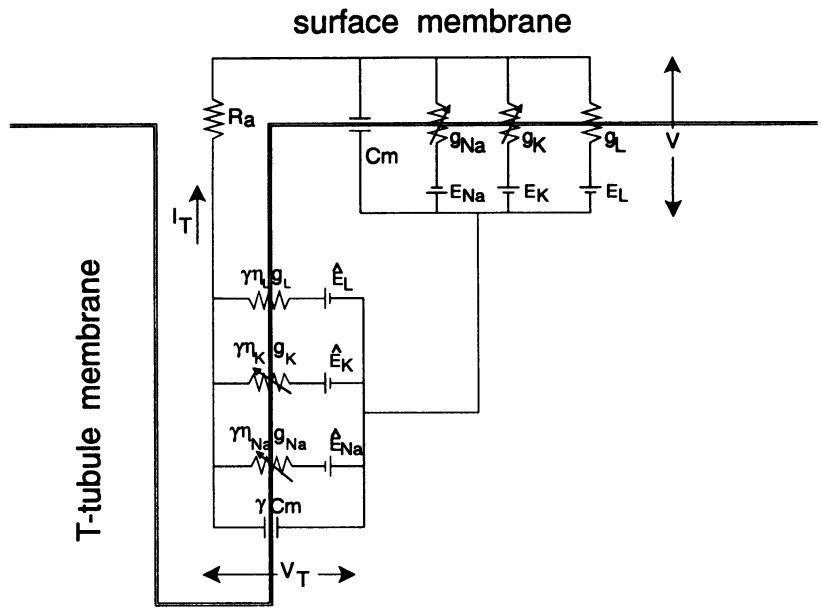

FIGURE 1 Equivalent circuit diagram for the model of the electrical behavior of a muscle fiber. The voltage and time dependence of the variable conductances are given by Eqs. 6, 7, 9, and 10. γ is the ratio of the T-tubular membrane area to surface membrane area. The ηs represent the density of ion channels in the T-tubular membrane relative to that of the surface membrane.

membrane may be expressed as

$$I_{ionic} = g_l(V - E_l) + g_{Na}(V - E_{Na}) + g_k(V - E_K) \quad (5)$$

where

$$g_{Na} = \bar{g}_{Na} m^3 h \quad (6)$$

$$g_K = \bar{g}_K n^4 \quad (7)$$

and the equilibrium potentials are defined by

$$E_l = \frac{RT}{F} \ln \frac{[K]_o + 0.01 \times [Na]_o}{[K]_i};$$

$$E_{Na} = \frac{RT}{F} \ln \frac{[Na]_o}{[Na]_i}; \qquad E_K = \frac{RT}{F} \ln \frac{[K]_o}{[K]_i} \quad (8)$$

We have set $[K]_o$ = 4.0, $[K]_i$ = 156, $[Na]_o$ = 150, and $[Na]_i$ = 24. Although the reversal potential for I_{leak} is dominated by a potassium-specific conductance in Eq. 8, it is not intended that the majority of this current is carried by K^+ ions in mammalian muscle. Most of the ionic current elicited at small deviations from the resting potential is carried by Cl^- ions (25). Equations 5 and 8 simply represent a mathematically convenient way to increase the slope conductance of the model cell in the vicinity of the resting potential and to have the reversal potential depend on $[K]_o$.

The Hodgkin-Huxley parameters m, h, and n are assumed to obey first-order kinetics such that

$$\frac{dy}{dt} = \alpha_y \times (1 - y) - \beta_y \times y; \quad y \in \{m, n, h\}. \quad (9)$$

The voltage dependence of the rate constants α and β is approximated as

$$\alpha_m = \frac{\bar{\alpha}_m (V - \bar{V}_m)}{1 - e^{-(V - V_m)/K_{\alpha m}}} \qquad \beta_m = \bar{\beta}_m e^{-(V - \bar{V}_m)/K_{\beta m}} \quad (10)$$

$$\alpha_h = \bar{\alpha}_h e^{-(V - \bar{V}_h)/K_{\alpha h}} \qquad \beta_h = \frac{\bar{\beta}_h}{1 + e^{-(V - \bar{V}_h)/K_{\beta h}}} \quad (11)$$

$$\alpha_n = \frac{\bar{\alpha}_n (V - \bar{V}_n)}{1 - e^{-(V - \bar{V}_n)/K_{\alpha n}}} \qquad \beta_n = \bar{\beta}_n e^{-(V - \bar{V}_n)/K_{\beta n}} \quad (12)$$

The ionic current flowing/unit area of T-tubule membrane is described by

$$\hat{I}_{ionic} = \eta_l \times g_l \times (V_t - \hat{E}_l) + \eta_{Na} \times g_{Na} \times (V_t - \hat{E}_{Na}) + \eta_K \times g_K \times (V_t - \hat{E}_K) \quad (13)$$

where η is the ratio of T-tubule-to-surface channel density and $\hat{E}$ is the reversal potential for a given channel across the T-tubule membrane. Because $[K]_t$ may vary as a consequence of ionic current flow, $[K]_t$ may not always equal $[K]_o$, and the reversal potentials for the potassium and the leak conductances may be different for the surface and T-tubule membranes.

The functional defect in the inactivation of sodium channels was modeled by setting h equal to 1 for a fraction of channels:

$$I_{Na} = (1 - f) \times \bar{g}_{Na} m^3 h (V - E_{NA}) + f \times \bar{g}_{Na} m^3 (V - E_{Na}) \quad (14)$$

where $0 \le f \le 1$ is the fractional proportion of noninactivating sodium channels. In terms of channel behavior, f equals the steady-state open probability at depolarized potentials, where $m \approx 1$ and $h \approx 0$. Although the patch-clamp results for HPP muscle from one family showed that f clearly increases with $[K]_o$ (6), the model computations herein used a fixed value of f for any given simulation. A constant f is analogous to a fixed concentration of ATX II in our in vitro model (17), so the model simulations can be compared to those experimental observations.

Accumulation of K^+ in the T-tubule

The model assumes that the T-tubule can be described as a spatially uniform compartment with a bulk K^+ concentration of $[K]_t$. The change in $[K]_t$ was approximated by the sum of a contribution due to potassium current flow across the T-tubule membrane and a diffusion term driven by $[K]_t$-$[K]_o$. Peachy has estimated a volume-to-surface-area ratio for the T-tubule as $\zeta = 10^{-6}$ cm (24). Thus the rate of change in $[K]_t$ due to the potassium current is

$$\frac{\hat{I}_K + 0.15 \times \hat{I}_l}{F \times \zeta} = \frac{\eta_K \times g_K \times (V_t - \hat{E}_K) + 0.15 \times \eta_l \times g_l \times (V_t - \hat{E}_l)}{F \times \zeta} \quad (15)$$

where F is Faraday's constant, and it has been assumed that 15% of the leak current is carried by K^+ ions. The diffusion of K^+ between the T-tubular space and the extracellular space is modeled as a passive (that is, voltage-independent) first-order rate process with a time constant τ_K. This time constant is determined experimentally by the half time for the recovery of the K^+ conductance after an extreme hyperpolarization (26) or by the half time for the decay in the after-depolarization which follows a train of repetitive discharges in a muscle fiber (21, 27). Both techniques estimate a half time of approximately 300–400 ms. For mammalian muscle, we have used a τ_K = 350 ms. The net rate of change in $[K]_t$ can be computed by combining these two processes as follows.

$$\frac{d[K]_t}{dt} = \frac{\eta_K \times g_K \times (V_t - \hat{E}_K) + 0.15 \times \eta_l \times (V_t - \hat{E}_l)}{F \times \zeta} - \frac{[K]_t - [K]_o}{\tau_K} \quad (16)$$

Selection of model parameters

One confounding feature of the model that potentially limits the interpretation of simulations is the large number of parameters. Fortunately, a reasonable degree of agreement exists within the body of reports published on the electrical properties of skeletal muscle. Furthermore, many of the major conclusions from the simulation, such as the stability of equilibrium potentials, the existence of repetitive firing, and the shifts in the resting potential, all arise as a consequence of the dynamical properties of the system equations and are not critically dependent on any one choice of parameter values.

The parameter values used in the computation of the ionic conductances are listed in Table 1 along with the references from which they were obtained. These values are representative for mammalian muscle, either rat or human. The sodium channel kinetics incorporate the major difference from amphibian muscle as described by Adrian and Marshall (28); steady-state activation was shifted in the hyperpolarizing direction such that half-maximal activation (m_∞^3 = 0.5) occurred at −40 mV. The 50% inhibition point for h_∞ occurred at a voltage of −80 mV and had a slope of −0.044 mV^{-1}. This slope is equivalent to a K_h of 5.65 mV in the exponent of a Boltzmann fit to $h_\infty(V)$. Temperature-sensitive parameters have been modified to their expected values at 22°C by assuming a Q_{10} of 2.5 for rate constants and a Q_{10} of 1.5 for conductances.

The only remaining free parameters are the ratios of the channel densities between the T-tubular and surface membranes. Although it is widely accepted that leakage, sodium, and potassium channels do exist in the T-tubule system, only limited measures of their density are available. The basis for our assumed values of these distributions is described in detail, because they have a profound effect on how the $[K]_t$-induced depolarization of the T-tubule membrane is propagated to the surface membrane. One technique for estimating the ratio of T-tubule to surface membrane channel density, η,

TABLE 1 Parameters for the gating variables, *m*, *h*, and *n* at 22°C

Parameter	value	units	Reference
$\bar{\alpha}_m$	0.288	ms^{-1}	29
$\bar{\beta}_m$	1.38	ms^{-1}	29
$\bar{V}_m$	−46	mV	22*
$K_{\alpha m}$	10	mV	22
$K_{\beta m}$	18	mV	22
$\bar{\alpha}_h$	0.0081	ms^{-1}	29
$\bar{\beta}_h$	4.38	ms^{-1}	29
$\bar{V}_h$	−45	mV	22‡
$K_{\alpha h}$	14.7	mV	29
$K_{\beta h}$	9	mV	22‡
$\bar{\alpha}_n$	0.0131	ms^{-1}	30
$\bar{\beta}_n$	0.067	ms^{-1}	30
$\bar{V}_n$	−40	mV	30
$K_{\alpha n}$	7	mV	30
$K_{\beta n}$	40	mV	30
	Conductances		
g_l	.75	mS/cm^2	25§
$\bar{g}_{Na}$	150	mS/cm^2	29
$\bar{g}_K$	21.6	mS/cm^2	30

* $\bar{V}_m$ was shifted from a value of −42 based on data in frog (22) so that $m_\infty^3 = 0.5$ at $v = -40$ mV as reported for rat (28).

‡ $K_{\beta h}$ and $\bar{V}_h$ were increased from the values of 7.6 and −41, respectively, in Adrian and Peachy (22) so that $h_\infty = 0.5$ at −80 mV and that the slope factor in a Boltzmann fit of $h_\infty(V)$ equaled 5.65 as reported by Almers et al. (31).

§ g_l was chosen such that the total membrane conductance in the vicinity of the resting potential equaled 2 mS/cm^2 as reported for rat muscle by Palade and Barchi (25).

is to compare the binding of channel-specific toxins before and after detubulating the fiber osmotically. Jaimovich et al. (32) reported that in frog muscle a 50% reduction in TTX binding results from detubulation. When combined with the estimate of the ratio between the surface area of T-Tubule and surface membrane, $\gamma = 4.8$ (24), the binding study implies that the relative density of sodium channels is $1/\gamma$ in the T-tubule compared to the surface membrane or η_{Na} equals 0.21. Caillé and colleagues (33) used frog semitendinosus in a double sucrose gap apparatus and rapid bath exchanges with TTX or low-Na^+ saline or detubulation to dissect out a sodium current contributed by the T-tubule system. The peak amplitude of the T-tubule component was about 20% of the surface Na^+ current. If it is assumed that the T-tubule membrane was well clamped, then the sodium channel density would be predicted to be severalfold lower than the value from the binding data. Adrian and Peachy used a value of 0.05 in their model (22). We have chosen an intermediate value of $\eta_{Na} = 0.1$.

Even less information is available for the estimate of η_K. Palade and Barchi (25) reported that the potassium contribution to the steady-state conductance of rat muscle appears to reside totally in the surface membrane. The range of test potentials they used, however, may not have activated the delayed rectifier in the T-tubule. Conversely, in amphibian muscle Eisenberg and Gage (34) showed that about 67% of the total potassium conductance resides in the T-tubules. Since it is reasonable to assume that $\bar{g}_K n^4 \ll g_a \equiv 1/R_a$ near V_{rest}, then the access resistance can be neglected and the total K^+ conductance is simply the sum of the surface and T-tubule contributions, $\bar{g}_K n^4 + \gamma\eta_K \times \bar{g}_K n^4$, respectively. Therefore the spatial distribution of the K^+ conductance reported for frog implies that

$$0.67 = \frac{\gamma\eta_K \times \bar{g}_K n^4}{\bar{g}_K n^4 + \gamma\eta_K \times \bar{g}_K n^4} = \frac{\gamma\eta_K}{1 + \gamma\eta_K} \tag{17}$$

and since $\gamma = 4.8$, then $\eta_K = 0.42$. Adrian and Peachy used a channel density ratio of 1/33 for surface to T-tubule potassium in their model (22). We have chosen an intermediate value of 0.4 so that $[K]_t$ increases by about 0.2 mM for each action potential.

η_l may be estimated from two different experimental results. In the vicinity of the resting potential, the total ionic conductance of a fiber is dominated by the contribution of the leak component. Palade and Barchi showed that in rat muscle about 70% of this conductance is lost in detubulated fibers and that the leak current is carried primarily by Cl^- ions (25). If it is assumed that the access conductance, g_a, is much larger than the leak conductance contributed by the T-tubule, then the leak conductances of the two membrane compartments are in parallel and their contributions add. By analogy to the computation for the K^+ conductance in Eq. 17, if the T-tubule system accounts for 70% of the total leak conductance, then $\eta_l = 0.5$. In contrast Eisenberg and Gage demonstrated that in frog muscle the majority of the leak current is carried by the surface membrane with almost no contribution from the T-tubule system (34).

This difference in the spatial distribution of the leak conductances is critical in determining the effect of T-tubule K^+ accumulation on V, the potential of the surface membrane. This effect is also the basis for the second piece of experimental evidence in favor of a value of $\eta_l \approx 0.5$. Freygang and colleagues (27) and Adrian and Bryant (21) showed that an afterdepolarization of about 1 mV/discharge persists for several hundred milliseconds following a train of 1 to 15 repetitive discharges. The afterdepolarization is abolished by detubulation and has been proposed to be caused by K^+ accumulation in the T-tubule. The increase in $[K]_t$ that must occur to cause V to depolarize by 1 mV is directly dependent on the value of η_l. Consider the simplified model of Fig. 2. This circuit approximates the behavior of the fiber for small and slow deviations from the resting potential where the leak currents dominate over all other ionic currents and the capacitive current is negligible. The after-depolarization occurs, because tubular K^+ accumulation shifts $\hat{E}_l$ which in turn depolarizes V, the surface membrane potential. The circuit forms a voltage divider, and V may be expressed as a weighted average of the two batteries which represent the reversal potentials for the leak currents in the surface and T-tubule membranes

$$V = \left[\frac{g_a + \hat{g}_l}{g_a\hat{g}_l + g_a g_l + \hat{g}_l g_l}\right] \times \left[g_l E_l + \left(\frac{g_a\hat{g}_l}{g_a + \hat{g}_l}\right)\hat{E}_l\right]. \tag{18}$$

The change in V due to a shift in $\hat{E}_l$ is

$$\Delta V = \left(\frac{\partial V}{\partial \hat{E}_l}\right)\Delta\hat{E}_l = \left(\frac{g_a\hat{g}_l}{g_a\hat{g}_l + g_a g_l + \hat{g}_l g_l}\right)\Delta\hat{E}_l. \tag{19}$$

Since $g_a \gg g_l$ or $\hat{g}_l$, then

$$\Delta V \approx \left(\frac{\hat{g}_l}{\hat{g}_l + g_l}\right)\Delta\hat{E}_l = \left(\frac{\gamma\eta_l}{\gamma\eta_l + 1}\right)\Delta\hat{E}_l \tag{20}$$

because we defined the T-tubule conductance/cm^2 of surface membrane as $\hat{g}_l = \gamma\eta_l g_l$. Adrian and Marshall have estimated that $[K]_t$ increases by 0.15–0.35 mM after a single action potential (20). Thus $\hat{E}_l$ will depolarize by up to approximately 1.5 mV, and V will depolarize by 1 mV if = 0.42. This value of η_l implies that 71% of the total leak conductance is contributed by the T-tubule membrane and agrees with our previous estimate based on the conductance change caused by detubulation.[1]

[1] It is worth noting that Eq. 20 shows why ΔV will be only a fraction of ΔE_l. Furthermore, because the dependence on η_l is hyperbolic, $\partial V/\partial\hat{E}_l$ falls off precipitously as η_l decreases from 0.5, and extraordinarily high values of η_l are required for $\partial V/\partial\hat{E}_l$ to approach 1.0. This illustrates a problem with hypothesis that K^+ accumulation in the T-tubule causes the afterdepolarization in amphibian muscle. In that preparation only about 18% of the total conductance is contributed by the T-tubule membrane (34) so that E_l must shift by 5.6 mV to depolarize V by 1 mV. The rise in $[K]_t$ required to produce this shift as a consequence of a single action potential seems excessive.

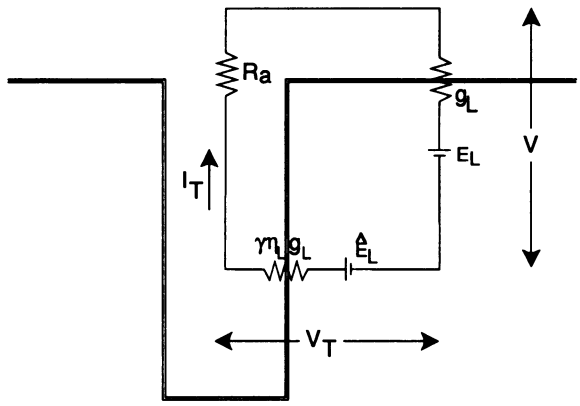

FIGURE 2 Electrical model for a quiescent muscle fiber. This approximation is valid when the system is both in steady state and at hyperpolarized potentials where the leak conductances dominate all other ionic conductances.

METHODS

Computation of model responses

All computations were performed on a 486-based personal computer (Northgate, Minneapolis, MN) which was programmed using the QuickBASIC environment (Microsoft, Redmond, WA). V and V_t were computed by numerical integration of the coupled differential equations in Eqs. 3 and 4. The initial conditions (resting surface and T-tubule potentials) were determined by setting the differentials in Eqs. 3 and 4 to zero and iteratively adjusting V until the net membrane current balanced the applied current. When the computation of the ionic currents are considered explicitly as in Eqs. 5–7 and 9 as well as the change in $[K]_t$ in Eq. 16, the complete system consists of nine coupled first-order nonlinear differential equations. Euler's method of integration was used with a variable time step. The maximum Δt was set at 0.1 ms unless otherwise noted. This value was reduced by a factor of 2 whenever $\Delta V \equiv (dV/dt)\Delta t$ exceeded a threshold of 0.5 mV, and a submaximal Δt was increased two-fold when ΔV was less than the voltage threshold. The existence of oscillations in the solution to the system equations can be predicted explicitly on theoretical grounds and was not dependent the size of Δt. Simulation of a single 300-ms run required approximately 4 min of computation time.

Voltage transients in rat muscle fibers

The in vitro model for myotonia in normal rat muscle has been presented elsewhere (17). Briefly, the extensor digitorum longus was dissected from the hind leg of an acutely decapitated rat and kept at room temperature in an oxygenated and bicarbonate-buffered saline bath. Transmembrane voltage was recorded from single fibers with a 3 M KCl-filled microelectrode, and stimulating currents were passed by a 2 M potassium citrate-filled microelectrode placed 40–80 μm from the recording electrode. A partial loss of sodium channel inactivation was induced by adding micromolar amounts of anemone toxin to the saline bath. *d*-Tubocurare (10 mg/liter) was added to block acetylcholine-induced responses evoked by the effects of anemone toxin on nerve endings. The proportion of noninactivating I_{Na} at a particular toxin concentration was determined in a sacrolemmal bleb preparation by measuring the steady-state open probability of unitary currents during prolonged depolarizations.

RESULTS

Simulation of normal muscle

The resting potential of a simulated fiber was −85 mV when $[K]_o$ was at a baseline value of 4.0 mM, and the ambient temperature was set to 295 K. This potential is determined primarily by the reversal potential of the leak current (−85.0), because that conductance dominates over all other ionic conductances. The current-voltage relationship in steady state is shown in Fig. 3. For this simulation, potassium accumulation in the T-tubule was disabled so that the model would approximate the I_m-V relationship observed experimentally in voltage-clamped fibers at quasi-steady state; that is, a few hundred milliseconds after the voltage step. The slope conductance equaled 2.2 mS/cm^2 at the resting potential. The contribution of each individual current is depicted by the light lines and shows that the majority of the resting conductance was due to I_t. Near the resting potential, I_t was produced mainly by current through the leak conductance in the T-tubule membrane. Approximately 70% of the resting conductance was contributed by the T-tubule because of the choice in parameters for the relative density of the leak conductance in the T-tubule membrane, η_l, and the amount of T-tubule membrane electrically coupled to a unit area of surface membrane, γ. The slope conductance initially decreased as V was depolarized and then sharply increased when the K^+ conductance was activated near −48 mV. This initial decrease in the total membrane conductance was caused by a small inward Na^+ current which occurred because there was a nonzero overlap in the voltage dependence of steady-state inactivation and activation, $h_\infty(V) \times m_\infty(V)^3$, even in a normal fiber. In the absence of external current injection, there was only one possible equilibrium potential, where $I_m = 0$. This locus determined the resting potential and was mathematically stable.

The model behavior to brief and long-duration current injection is compared to responses recorded from rat fast-twitch muscle in Fig. 4. The subthreshold responses decayed

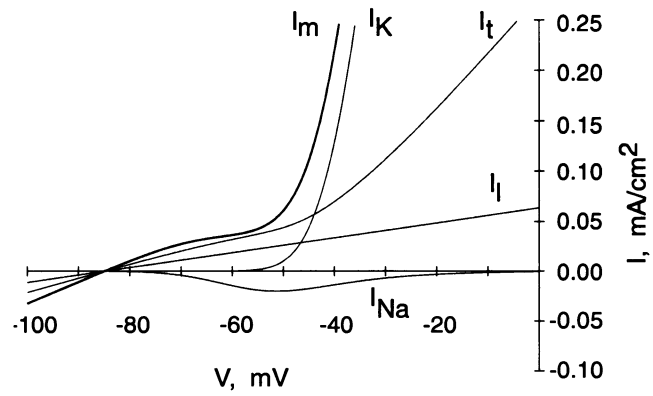

FIGURE 3 Current-voltage relationship for the model of a muscle fiber. The dark line shows the total ionic current for 1 cm^2 of surface membrane. Lighter lines depict individual ionic components of the surface current. I_m was computed at each V from Eq. 3. At a given value for V, V_t was determined by iterative approximation until Eq. 4 was satisfied.

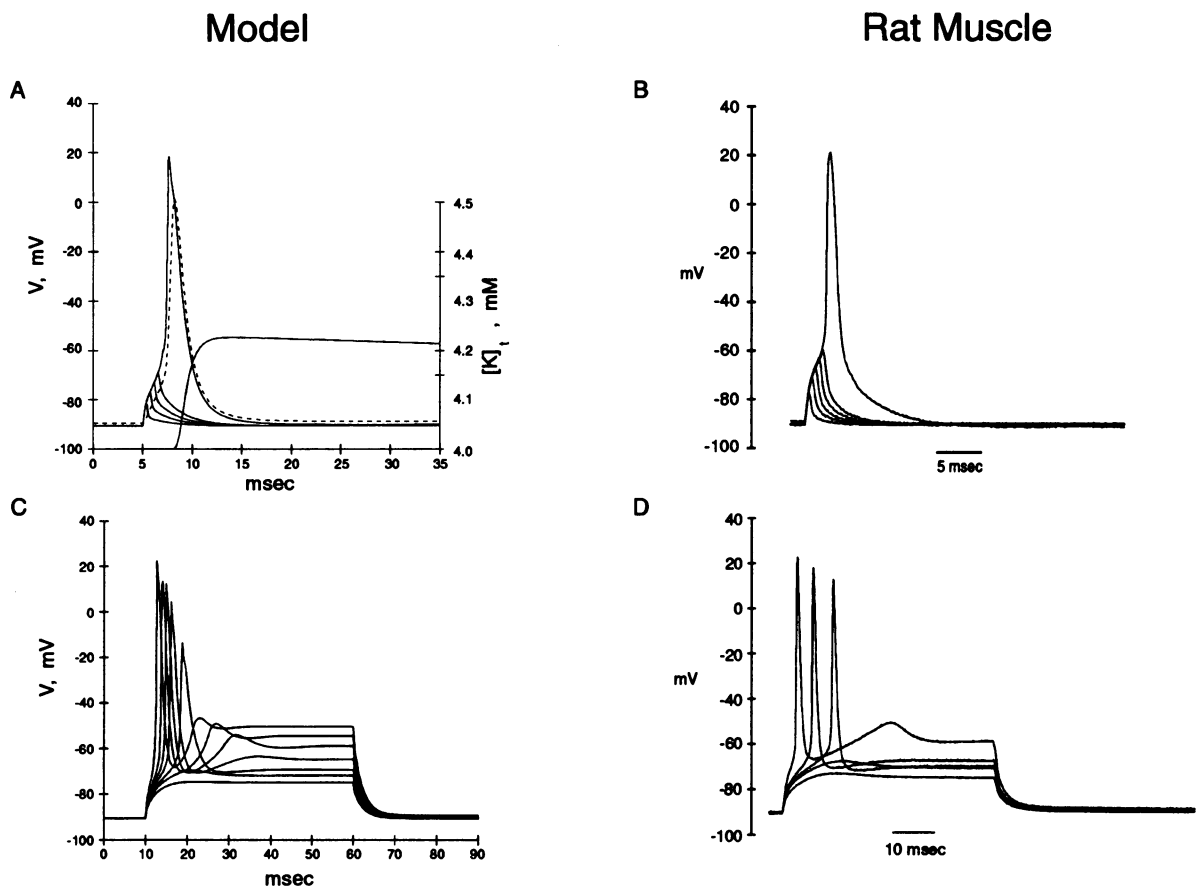

FIGURE 4 Model and rat muscle responses to short and long-duration current injection. For the simulations, the normal parameter values listed in Table 1 were used. Each response starts from a holding current of -12 μA/cm^2 to set the resting potential at -90 mV. A holding current was applied to the rat muscle fibers so that V_m was set to -90 mV before the application of the stimulus current. (*A*) Model responses are superimposed for four subthreshold and one suprathreshold stimulation. Stimulus intensity was 60 μA/cm^2, and the duration was varied in steps of 0.4 ms from 0.4 to 2.0 ms. The dashed line shows the membrane potential of the T-tubule, V_t, for the suprathreshold response. V and V_t do not start from the same value because of the presence of the holding current. [K] accumulates in the T-tubule during the suprathreshold responses and peaks at 4.22 mM. (*B*) Membrane voltage transients were recorded from rat fibers stimulated with a 200-nA current pulse applied over a range of durations from 0.4 to 2.4 ms in steps of 0.4 ms. (*C*) Surface membrane potential, V, is shown for a series of 50-ms current stimulations spanning the range from threshold (28 μA/cm^2) to 2 $\times$ threshold (56 μA/cm^2). Only a single action potential is elicited, even with the largest stimulus intensity. Stimulus intensities were 20, 25, 28, 32, 36, 42, and 56 μA/cm^2. (*D*) Muscle fibers fired only a single spike in response to long-duration current stimuli of up to 1.5 $\times$ threshold. For this fiber, threshold was 115 nA; responses to stimuli of 90, 110, 115, 130, and 175 nA are shown.

with a two exponential time course for both the model (Fig. 4 *A*) and the rat muscle (Fig. 4 *B*). The decay was not monoexponential, because the surface membrane relaxes more quickly from a subthreshold depolarization than the T-tubule membrane. For the limiting case where the two membrane compartments are completely decoupled ($g_a = 0$), the surface membrane has a time constant of C_m/g_L which is smaller than that of the T-tubule membrane, $(C_m/\eta_l g_l)$.

The potential difference across the T-tubule, V_t, is shown as a dashed line for the suprathreshold response. Depolarization of the T-tubule membrane lagged behind that of the surface membrane because the access resistance, R_a, reduced the current available to depolarize V_t and the T-tubular membrane had a larger time constant. This slowed inward current caused the subtle inflection in the initial decent of V during the repolarizing phase of the action potential. The peak depolarization of V_t during an action potential was strongly dependent on the density of Na^+ channels in the T-tubule membrane, η_{Na}, and the access resistance, R_a. For values of η_{Na} larger than 0.5, the peak depolarization nearly equaled $\hat{E}_{Na}$. If R_a was constrained to the value of 150 Ω-cm^2 as suggested by Adrian et al. (23), then with η_{Na} larger than 0.1, the depolarization of V_t approached or even exceeded that of V. When this occurred, the inflection during the repolarization phase of V became more pronounced or even created a second local peak. However, this glitch in the falling phase of an action potential was not observed experimentally, and thus the maximum allowable value of η_{Na} is limited to 0.1 in our model. A higher density of Na^+ channels in the T-tubule membrane may be acceptable in a model using a distributed network for the T-tubule compartment.

The accumulation of K^+ in the T-tubule during a single action potential is shown in Fig. 4 *A*. This 0.2 mM increase

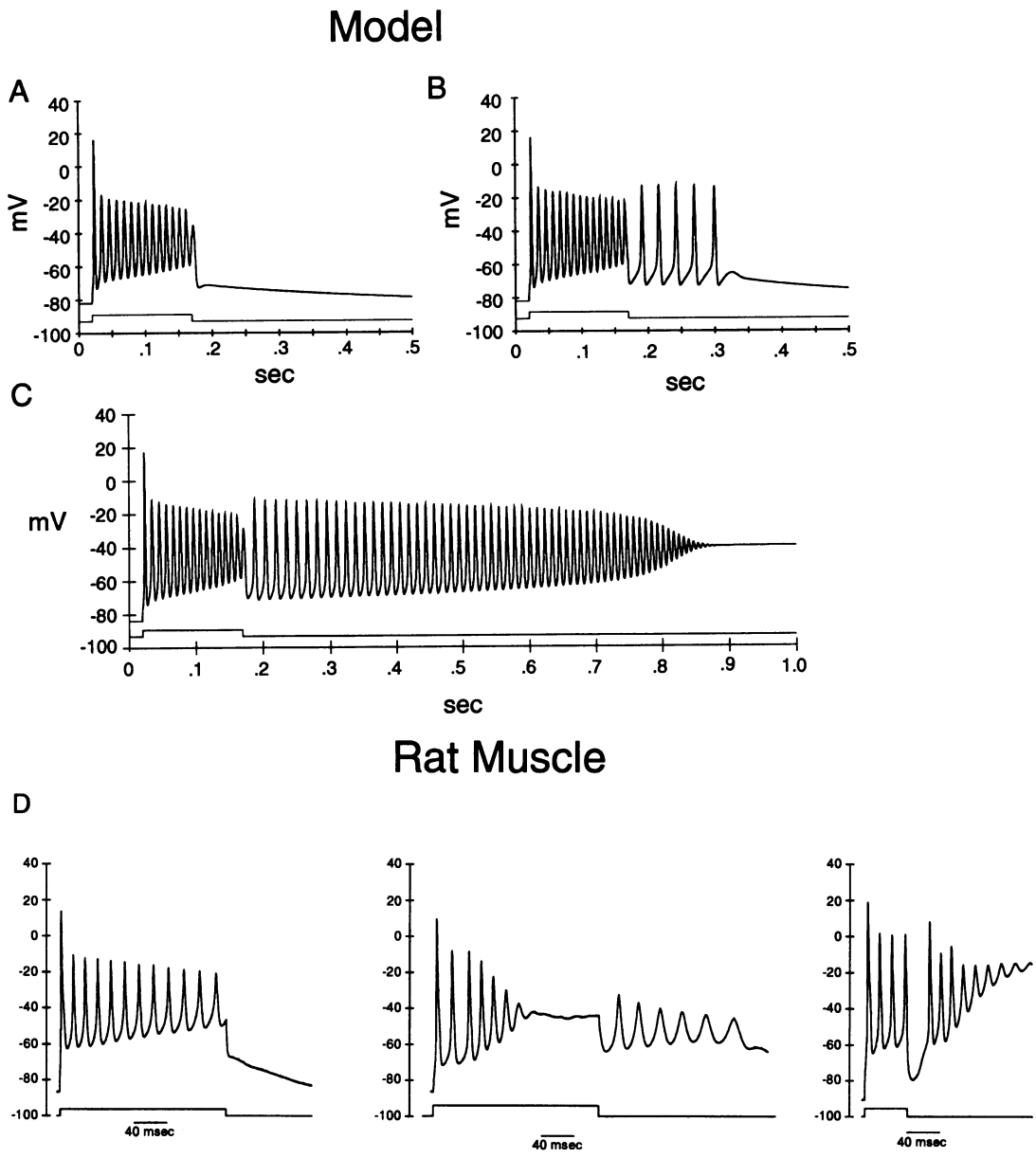

FIGURE 5 Myotonic discharges computed when noninactivating Na^+ channels were incorporated into the model or when muscle fibers were exposed to ATX II. A current pulse of 1.5 × threshold (45 μA/cm2) was applied for 150 ms in each simulation. The proportion of noninactivating Na^+ channels, f, was varied as follows: (*A*) 0.015, (*B*) 0.018, (*C*) 0.02. At the end of the stimulus interval, $[K]_t$ had increased to 9.4, 11.0, and 12.0 mM, for the three respective values of f. All other parameters are set to their normal values as listed in Table 1. (*D*) In 10 μM ATX II, suprathreshold current stimuli elicited repetitive discharges which were followed at the end of the stimulus by an after-depolarization or sometimes after-discharges. In some fibers, repetitive discharges progressed to a stable depolarization of the membrane. For these three different fibers, the current intensities were (left to right) 90 nA (2 × threshold), 75 nA (1.5 × threshold), and 80 nA (1.3 × threshold).

in $[K]_t$ was comparable to the value estimated by Adrian and Marshall (20), and caused an after-depolarization of the surface and T-tubule membranes of 0.7 and 0.9 mV, respectively.

The model and rat muscle responses to a long-duration stimuli is shown in Fig. 4, *C* and *D*. A threshold stimulus elicited a single action potential in both systems. Stimuli of 1.5 or even two times threshold also elicit a single action potential. There was, however, an attenuated depolarizing wave after the spike. These features were also present in suprathreshold responses for the rat fibers.

Simulation of muscle with a small proportion of noninactivating Na^+ channels

Response to long-duration current stimuli

Noninactivating Na^+ channels were incorporated into the model by fixing the inactivation variable, h, equal to 1 for a small fraction, $0 \leq f \leq 1$, of the total pool of channels. The original resting potential did not shift when noninactivating Na^+ channels were introduced. Similarly, when ATX II caused a steady-state open probability of up to 0.02, there was no spontaneous depolarization of the

membrane (17). As described below, however, a perturbation in V from the resting potential may cause the system to relax to a new equilibrium potential. These additional equilibrium potentials, both stable and unstable, occur when $f > 0$. The stimulus threshold to fire an action potential was not significantly reduced by the presence of noninactivating Na^+ channels ($0 < f < 0.1$), and the latency to firing was not increased at the threshold intensity. In contrast, the responses in the low g_{Cl} fibers of the myotonic goat had a reduced current threshold and an increased latency to discharge at threshold (21). Even in normal rat muscle, a small probability exists that a sodium channel will reside in the open state long after the membrane is depolarized (17). This small value of $f = 0.001$, however, did not change the response to long-duration current injection. Only a single action potential was elicited and the response was indistinguishable from that in Fig. 4 *C*.

Simulations with long-duration current injection are shown in Fig. 5 for three different proportions of noninactivating Na^+ channels, f. When f was greater than 0.0075, suprathreshold stimuli produced a train of discharges during the stimulus interval. Activity-dependent accumulation of T-tubular K^+ caused a progressive depolarizing shift which was apparent at the end of each successive action potential. Because the vast majority of Na^+ channels inactivated normally, the depolarizing shift caused a progressive attenuation in the amplitude of the repetitive spikes. The frequency of the spikes also increased during the stimulus as a consequence of the K^+ accumulation.

The response at the end of the stimulus was variable and depended on f and $[K]_t$. For small values of f, the discharges did not continue after the end of the stimulus period. The poststimulus response was an after-depolarization that decayed back to the baseline resting potential with a time constant equal to τ_K (Fig. 5 *A*). The initial amplitude of the after-depolarization was 0.7 times the shift in $\hat{E}_1$, as expressed in Eq. 20.

When f equaled 0.018, a 150-ms current injection caused sufficient K^+ accumulation in the T-tubule for a train of spikes to persist beyond the termination of the stimulus. The tubular K^+ accumulation was greater, because with the larger value of f, more spikes occurred during the 150-ms stimulus, and the amplitude of each discharge was greater. In this particular simulation, $[K]_t$ had risen to 11.0 mM when the current injection ended. The after-depolarization was then large enough to trigger a series of discharges (Fig. 5 *B*). The frequency of spikes, however, was low enough relative to rate of the decay in $[K]_t$ so that each successive action potential raised $[K]_t$ by less than the diffusional loss. Eventually $[K]_t$ fell below a threshold, and V decayed exponentially back to the baseline resting potential and $[K]_t$ returned to the bulk extracellular value of 4.0 mM.

Fig. 5 *C* shows a simulation in which the after-discharges caused a progressive increase in $[K]_t$. The progressive depolarization of $\hat{E}_1$ caused the discharges to occur at increasingly higher frequency. This same depolarizing shift inactivated more and more of the normally inactivating Na^+ channels as indicated by the progressive reduction in the amplitude of the after-discharges. Eventually, there was not a sufficient Na^+ current to generate any spike, and V reached a new steady-state at a potential markedly depolarized from the initial resting potential. In this state, the model was refractory to firing any further spikes, even with current injection; it corresponds to the flaccid paralysis that occurs in patients with periodic paralysis. When the model settled to a stable depolarized potential, as in Fig. 5 *C*, it remained there and did not repolarize unless a hyperpolarizing stimulus was applied. Once the $[K]_t$-induced depolarization was sufficient to activate Na^+ channels, V was essentially independent of $[K]_t$. It was determined by a balance of currents carried by the noninactivating I_{Na} and I_K of the sarcolemma. $[K]_t$ continued to rise and, after several seconds, asymptotically approached 39 mM. This value of $[K]_t$ is unlikely to occur physiologically and illustrates a limitation of the model. In skeletal muscle, elevated extracellular [K] shifts the voltage dependence of gating for the inward rectifier, and increased $[Na]_i$ stimulates the Na/KATPase. These and other mechanisms limit the elevation of $[K]_t$ and contribute to recovery from a depolarized plateau potential, but are beyond the scope of the present model.

Since the poststimulus response depended on the combination of f and $[K]_t$, then even with a fixed value of f the behavior depended on the stimulus. For example, when $f = 0.018$, a limited train of spikes occurred after a 150-ms current injection, and V returned to the baseline resting potential, as in Fig. 5 *B*. For a 100-ms stimulus no after-discharges occurred and the response was of the form in Fig. 5 *A*. Conversely, a 200-ms stimulus evoked a train of discharges with progressively increasing frequency, and eventually V settled at a depolarized equilibrium potential as in Fig. 5 *C*. The difference in these three cases was the value $[K]_t$ had attained by the end of the stimulus period.

These three forms of after-response were observed in rat muscle when steps of depolarizing current applied to fibers exposed to 10 μM ATX II (Fig. 5 *d*). At that toxin concentration, the Na^+ channel steady-state open probability, which is numerically equivalent to f in the model, was 0.018 ± 0.003 (17).

Effects of detubulation

In several experimental preparations it has been established that an intact T-tubular system is required for the production of myotonic runs of discharges continuing after the termination of the current injection (17, 21). This is a requirement for both the low-chloride conductance and the noninactivating sodium-channel mechanisms of myotonia. Detubulation was introduced into the model by increasing the access resistance, R_a. Complete electrical decoupling of the surface and T-tubular membranes occurs when R_a approaches infinity. Such a drastic increase, however, also causes a loss of 70% of the leak conductance because of the distribution of the leak conductance in mammalian fibers ($\eta_l = 0.5$). Loss

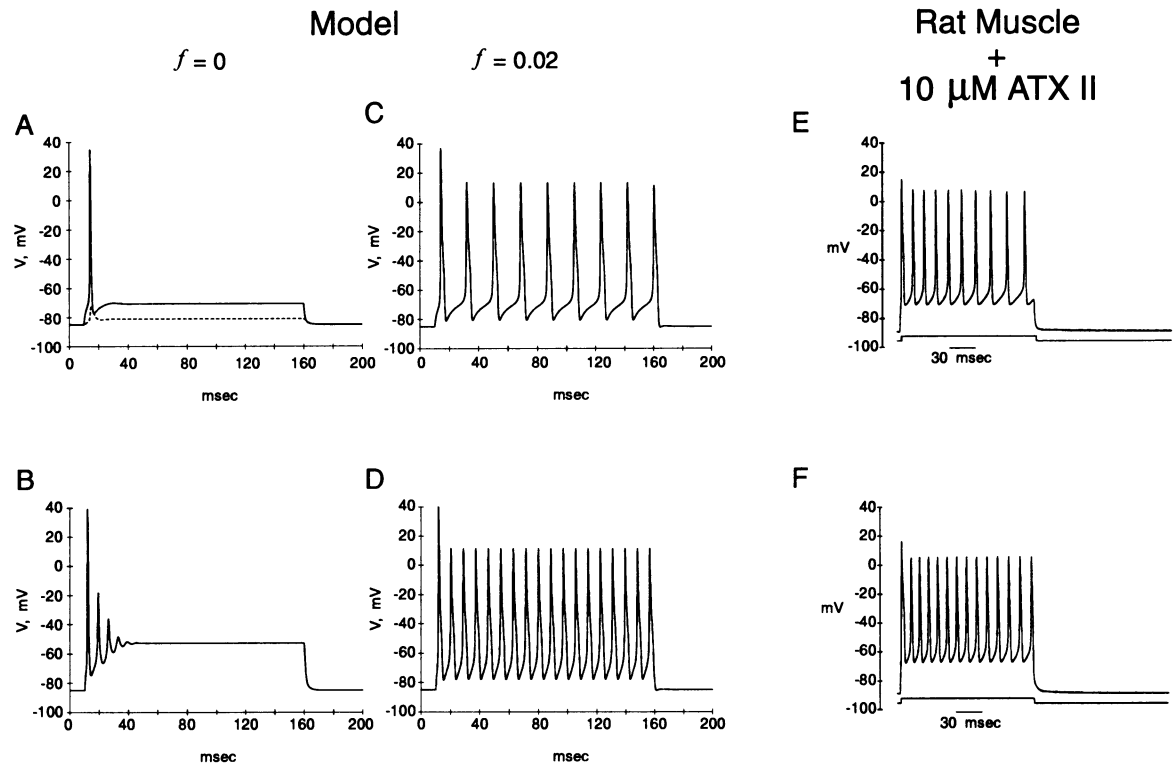

FIGURE 6 Responses in detubulated fibers. In the model, the access resistance was increased 10-fold to simulate detubulation. (*A*) A suprathreshold stimulus of 14 $\mu A/cm^2$ produced a single action potential on the surface membrane (*solid line*) and a subthreshold depolarization of 14 mV in the T-tubular membrane (*dashed line*). (*B*) The electrical decoupling of detubulation reduced the leak conductance by 70% so that 2 × threshold stimuli (24 $\mu A/cm^{2)}$ produced a partially myotonic response even with a completely inactivating Na^+ conductance. With a partially noninactivating Na^+ conductance, $f = 0.02$, these same two stimulus intensities elicited the repetitive spikes in *C* and *D*. Rat muscle fibers were detubulated by a 1-h exposure to 400-mOsm glycerol. (*E*) A suprathreshold current stimulus of 70 nA (1.75 × threshold) elicited repetitive discharges during the injection, but neither peristimulus depolarizing shifts, after-depolarizations, nor after-discharges occurred. (*F*) Stimulation with higher intensity current pulses (90 nA) elicited discharges with a higher frequency, but no after responses. When a partial loss of sodium channel inactivation occurred in detubulated fibers from either the computer model or the rat muscle, then suprathreshold stimuli elicited trains of discharges during the stimulus, but there was no progressive depolarizing shift in *V*, after-depolarization, or after-discharges.

of the leak conductance alone induces a myotonic state, even without incorporating noninactivating sodium channels. As shown by Adrian and Marshall in their model for the myotonia produced by a low chloride conductance (20), a 70% reduction in the leak conductance caused the surface membrane in our model to discharge repetitively during long-duration current injection. Palade and Barchi have commented that glycerol treatment is only partially successful in detubulating fibers as assessed by a change in apparent membrane capacitance (25). We modeled such a partial detubulation by increasing R_a 10-fold to 1500 Ω-cm^2. This value of R_a decoupled the system sufficiently to prevent large depolarizations and K^+ accumulation in the T-tubule and reduced the slope conductance of the I_m-V relationship from 2.2 to 1.3 mS/cm^2. In addition, the threshold current intensity was reduced by about 50%. Only a single discharge occurred for stimuli from 1.0 to 1.25 × threshold (Fig. 6 *A*). A triplet of damped action potentials occurred for larger stimulus intensities of 1.7× threshold or higher (Fig. 6 *B*). The depolarization in the T-tubule membrane during a surface action potential was only 14 mV, and $[K]_t$ did not change. The decoupling of the sarcolemma from the T-tubular membrane with its associated longer time constant caused a reduction in the duration of the surface action potential.

Noninactivating sodium channels tremendously enhanced the myotonic features of the partially detubulated model. A train of repetitive spikes occurred during the stimulus whenever f exceeded 0.0045. After-discharges, however, never occurred with partial detubulation. To maximize the likelihood of producing after-discharges, simulations were performed with a relatively large proportion of noninactivating sodium channels, $f = 0.02$, and with current intensities of 1 × and 2 × threshold applied for 150 ms. The responses in Fig. 6, *C* and *D*, show that a train of uniform amplitude spikes occurred during the stimulus but no after discharges were observed. The response in a detubulated rat muscle fiber with disrupted inactivation (10 μM ATX II) is shown for two different stimulus intensities in Fig. 6, *E* and *F*. Just as in the model simulation, there was no cumulative depolarizing shift during the train of spikes and there was no after-response.

Detubulation had four effects. 1) The T-tubule membrane was never significantly depolarized by the surface spikes. 2) No K^+ accumulation occurred in the T-tubular space. 3) Any

change in the reversal potential for the leak or K^+ conductance of the T-tubular membrane did not influence V significantly, as expressed in Eq. 19.[2] 4) The effective capacitance for the entire fiber was reduced. Therefore, in the simulation of even partially detubulated fibers, there was no progressive depolarizing shift at the end of each discharge, no variation in the amplitude of the repetitive discharges during the stimulus, and no slower phase of repolarization of V at the end of the stimulus. No after-depolarization or after-discharges occurred. These features all require an intact T-tubule system and the depolarizing influence it exerts after repetitive activity. The specific mechanism is most likely an accumulation of K^+ in the T-tubular space. In addition, the reduced capacitance caused a reduction in the duration of action potentials on the surface membrane. All of these features were also evident in the responses recorded from detubulated muscle fibers (17).

Response to short-duration current stimuli

The model response to a brief suprathreshold stimulus, with the T-tubule compartment intact, is shown in Fig. 7 for varying proportions of noninactivating Na^+ channels. The persistent Na^+ current increased the duration of the action potential, and if f was large enough, caused the system to settle at a depolarized equilibrium potential. Values of f from 0.01 to 0.02, that were sufficient to cause trains of action potentials for long duration current injections, caused only a minute change in the duration of the action potential. Thus, as we observed in ATX II-treated rat muscle, the response to long-duration stimulation is a more sensitive index of noninactivating sodium channels than the duration of an action potential from a brief stimulus (Ref. 17, Fig. 6). It is also important to note, however, that only a rather modest increase in f, to $f \geq 0.07$, was required to cause the system to settle at a depolarized equilibrium potential after a single discharge. This degree of inactivation failure is comparable to that recorded from Na^+ channels in muscle biopsied from a patient with hyperkalemic periodic paralysis (6). Thus the model predicts that it is possible to progress from a state of normal action potential conduction to one of depolarization block without passing through a region of repetitive discharges with a slow accumulation of T-tubular K^+. The clinical correlate is that many patients with HPP experience attacks of flaccid paralysis without first passing through a period of myotonic stiffness.

Current-voltage relationship

The existence of the depolarized equilibrium potential that occurred with noninactivating Na^+ channels can be easily demonstrated from the I_m-V relation. A quasi-steady-state I_m-V curve is shown in Fig. 8 for a range of values of f. As in Fig. 3, it is quasi-steady-state, because $[K]_t$ has been fixed at a value of 4.0 mM. This simulates a condition in which all the initial current transients have settled, but $[K]_t$ has not risen significantly at depolarized potentials. With $f = 0$, only one equilibrium potential exists, and it is stable; that is, all transient responses eventually return to a V arbitrarily close to the intersection of the I_m-V curve with the ordinate. When $f > 0.0187$ then the inward sodium current caused the I_m-V curve to intersect the ordinate at three possible equilibrium potentials.[3] The left-most intersection is always a stable equilibrium and represents a possible steady-state value for V. The middle equilibrium potential is always unstable, and thus does not represent a possible resting potential. Finally, the right-most point of intersection may be either a stable or an unstable equilibrium potential, depending on the value of f. Although a second stable equilibrium potential may exist mathematically, the membrane potential may not settle to this new value during the course of an action potential. For example, Fig. 8 shows that multiple equilibrium potentials existed whenever f was greater than 0.018. The equilibrium potential at −85 mV was always stable and the right-most equilibrium potential was stable if f exceeded 0.047. Fig. 7 shows, however, that f must be 0.07 or greater in order for the repolarizing phase of an action potential to settle at the depolarized equilibrium potential.

In the complete model, therefore, it is not difficult to envision the existence of multiple equilibrium potentials from the I_m-V relationship, but it is not possible to predict which value the system will settle to at steady state. The model could be characterized by performing a large number of simulations (18), but it is more efficient and insightful to examine the global behavior of the system with a phase-plane analysis of a reduced model.

Phase-plane analysis of a reduced model

It is possible to simplify the model while retaining those elements that produce myotonic discharges or paralysis. Consider the behavior of the complete model in the region of most interest—the falling phase of the action potential (cf. Fig. 7). At this point the response diverges to either normal repolarization, repetitive firing, or stabilization at a depolarized equilibrium potential. Here the falling phase of the action potential is slower than the kinetics of activation for Na^+ channels so

$$m(V,t) \approx m_\infty(V) = \frac{\alpha_m(V)}{\alpha_m(V) + \beta_m(V)}. \qquad (21)$$

In this voltage range the normal Na^+ channels are almost fully inactivated so that $h(V,t) \approx 0$. This approximation constrains the system such that the Na^+ current will be passed solely by the noninactivating fraction of channels. Thus from

[2] $\partial V/\partial \hat{E}_l$ approaches 0 as $g_a = 1/R_a$ decreases.

[3] The minimum value of f required to cause multiple points of intersection between the I_m-V curve and the ordinate depended on $[K]_t$. Thus for values of $f < 0.018$ the system still may come to rest at a depolarized equilibrium potential, provided $[K]_t$ is large enough.

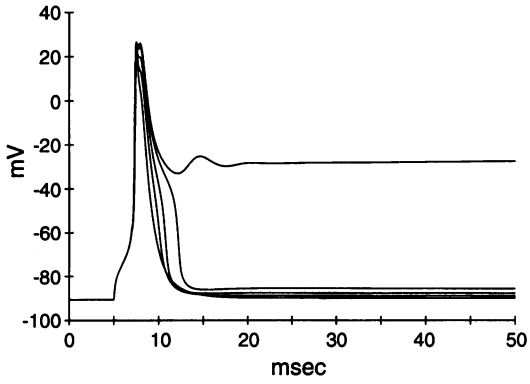

FIGURE 7 Model response to brief stimulation with varying proportions of noninactivating Na^+ channels. A holding current of -12 $\mu A/cm^2$ was applied to set $V = -90$ mV. The stimulus was a 60-mA/cm^2 pulse of 2-ms duration. The proportion of noninactivating Na^+ channels was increased over the range: $f = 0$, 0.02, 0.04, 0.06, 0.07. For larger values of f, the duration of the action potential progressively increased until a single stimulus caused the surface potential to settle at a depolarized equilibrium potential of -28 mV.

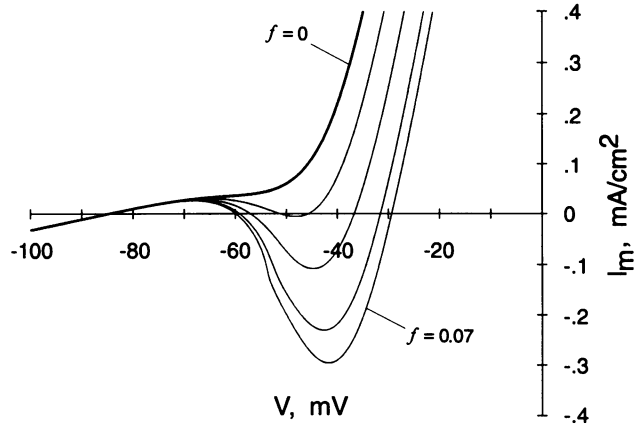

FIGURE 8 Quasi-steady-state current voltage relationship for various proportions of noninactivating Na^+ channels. The heavy line shows the sum of all currents passing through the surface membrane, I_m, as a function of transmembrane voltage for a normal fiber. The light lines show this relationship when a small proportion of the sodium conductance fails to inactivate: $f = 0.02$, 0.04, 0.06, 0.07. Larger values of f caused a greater dip in the I_m-V curve. For each curve, the right-most equilibrium potential was stable only when f was greater than 0.047. This second stable equilibrium potential caused the plateau depolarization shown in Fig. 7.

Eq. 21, the Na^+ current is defined as

$$I_{Na} = f \times \bar{g}_{Na} m_\infty^3 \times (V - E_{Na}). \quad (22)$$

Finally, the model was restricted to a space-clamped, single compartment of excitable membrane. The specific capacitance of this hypothetical patch of muscle surface membrane was increased from 1 to 4 $\mu F/cm^2$ to more closely approximate the dominant time constant of the electrically coupled surface and T-tubule membranes. For any particular simulation in the reduced model, $[K]_o$ remained constant. The previously described effects of $[K]_t$ accumulation can be represented in this reduced system by visualizing a slow transition across the results from many independent simulations with different fixed values of $[K]_o$. With these approximations, the reduced model simplifies from nine down to two coupled, nonlinear differential equations

$$\frac{dV}{dt} = \frac{1}{C_m}[I_m - f \times \bar{g}_{Na} m_\infty^3 \times (V - E_{Na}) - \bar{g}_K n^4 \times (V - E_K) - g_l \times (V - E_l)] \quad (23)$$

$$\frac{dn}{dt} = \alpha_n \times (1 - n) - \beta_n \times n. \quad (24)$$

Solutions to this reduced system of equations may be represented graphically in a single plane which allows a geometric interpretation of their behavior (35). Because the derivatives of $V(t)$ and $n(V,t)$ do not explicitly depend on time, t, the system is autonomous and has unique, nonintersecting trajectories in the n-V phase plane.

The voltage response of the reduced model to an impulse of depolarizing current is compared to that of the full model in Fig. 9 *A* (*top*). The rate of depolarization was slower, and the peak amplitude was smaller in the reduced model, because less Na^+ current was available to depolarize the membrane with $h = 0$. Nevertheless, the approximation was fairly accurate and the computation was simplified significantly. The time course of $n(V,t)$ also shows very little difference between the full and reduced models. The trajectory of an action potential in the n-V phase plane was constructed by plotting pairs of n and V at each time step, 0.1 ms (Fig. 9 *B*). The trajectory started at point *A*, the resting potential. The brief current pulse instantaneously depolarized the membrane to point *B*. n initially remained unchanged, because the activation of K^+ channels is not instantaneous. The Na^+ current through the noninactivating channels then caused the trajectory to continue further in the depolarizing direction. Simultaneously, K^+ channels were activated so n slowly increased and the trajectory turned upward. Eventually the outward potassium and leak currents balanced the Na^+ current, at point *C*, dV/dt equaled 0, and the trajectory began to move in the hyperpolarizing direction. This is the falling phase of the action potential. Repolarization continued and V returned to the resting potential at point *A*.

The general path of any trajectory in the n-V plane may be deduced geometrically by computing the derivatives specified by Eqs. 23 and 24. The n-nullcline represents all points where $dn/dt = 0$; n is constant, and any trajectory must be moving horizontally. The locus of these points is the familiar sigmoidal $n_\infty(V)$ curve which is drawn as a dashed line in Fig. 9 *B*. For all regions above this curve $dn/dt < 0$ and every trajectory must move downward. Conversely, at all locations below this curve $dn/dt > 0$, and the trajectory must move upward in the direction of increasing n. A second nullcline in the n-V plane is defined by the locus of all n, v pairs where $dV/dt = 0$. The V-nullcline was computed from Eq. 23 by

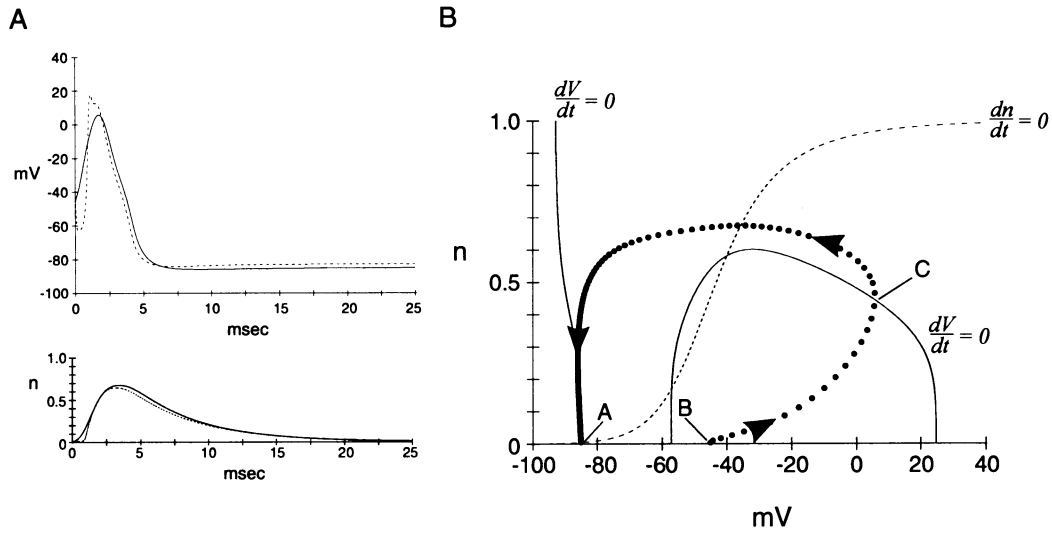

FIGURE 9 Action potential generated by the reduced model. (*A*) The membrane potential and K^+ channel activation parameter, n, are compared between the full model (*dashed lines*) and the reduced model with $f = 0.025$ in both. The response of the reduced model is qualitatively similar to that of the full one. (*B*) The response of the reduced model from (*A*) is replotted in the n-V phase plane. At every 0.1 ms, a pair of n and V values is plotted as a filled circle. The resting potential is at point *A*, a current pulse drives the system to point *B*, and the peak of the action potential occurs at point *C*. The dashed line shows the n-nullcline where $dn/dt = 0$ as defined by Eq. 24. The V-nullcline (*solid line*) was computed by setting $dv/dt = 0$ in Eq. 23. The two nullclines intersect at equilibrium positions. See text for details.

setting $dV/dt = 0$ and solving the fourth-order algebraic equation in n at any given V. These points lie on two branches of a curve in Fig. 9 *B*. Analogous to the argument for n, every trajectory must be moving vertically as it crosses the V-nullcline. At all locations to the left of and below the V-nullcline, $dV/dt > 0$ and trajectories course rightward in the depolarizing direction; the response is regenerative. In the region above the V-nullcline, $dV/dt < 0$, and trajectories moved in the hyperpolarizing direction. An appreciation of the significance of nullclines allows a geometric interpretation of threshold: the initial step depolarization in V must be large enough to cross the V-nullcline, otherwise the trajectory will relax back toward the resting potential without depolarizing further in the rightward direction. The other geometric constraint for the autonomous system of Eqs. 23 and 24 is that no trajectories intersect. These limitations on the possible paths for any arbitrary trajectory in the n-V plane allowed a rapid geometrical intuition for all trajectories after computing the path of a small number of examples.

Nullclines intersect at singularities where neither n nor V is changing, and thus these loci are equilibrium positions. They may be either stable or unstable equilibria. Stability was assessed at each equilibrium position by computing the eigenvalues of a first order approximation of Eqs. 23 and 24 in the neighborhood of the singularity (see Appendix). All local trajectories approach stable singularities as time proceeds. The approach may be asymptotic or spiral, for real- or complex-valued eigenvalues, respectively. In the n-V phase plane, the singularity at point *A* (Fig. 9 *B*) was always a stable node with negative real-valued eigenvalues. With this mathematical characterization of an equilibrium potential, a generalized description for the behavior of the membrane voltage can be stated without having to perform an exhaustive set of simulations: after any current pulse, the membrane voltage will approach the resting potential monotonically without ever oscillating about this voltage.

The repertoire of possible behaviors of the reduced model can be determined by computing how the equilibrium points shift and change in stability character as either f or $[K]_o$ is varied. Families of nullclines were computed to generate phase portraits for different proportions of noninactivating Na^+ channels, f, at two different fixed values of $[K]_o$. First, consider the case shown in Fig. 10 where the extracellular [K] remained equal to 4 mM. Since $n(V)$ does not explicitly depend on f (Eq. 24), the n-nullcline does not shift as f is varied. Also notice that the left-hand branch of the V-nullcline is insensitive to changes in f, leaving only the right branch of the V-nullcline to vary. The eigenvalues were computed at each equilibrium potential, and the stability of each locus is indicated by a particular symbol. Filled circles indicate real-valued eigenvalues that are negative and correspond to stable nodes. All local trajectories move toward a stable node without spiraling around it. The correlate in the time domain is a monotonic approach to an equilibrium potential without any oscillations. Open triangles indicate equilibrium potentials that were unstable saddles. The eigenvalues at these loci were also real-valued, but one was greater than zero and created the instability. Local trajectories veered away from an unstable saddle as time progressed without wrapping around it. Thus again, the temporal course was nonoscillatory. The squares mark equilibrium potentials that had complex-valued eigenvalues. This created a focus, either stable or unstable, which produced a spiral in the phase plane and oscillations in the time domain. A focus was stable when the real part of the eigenvalue was less than zero and these points are shown as filled squares. A local trajectory spiraled

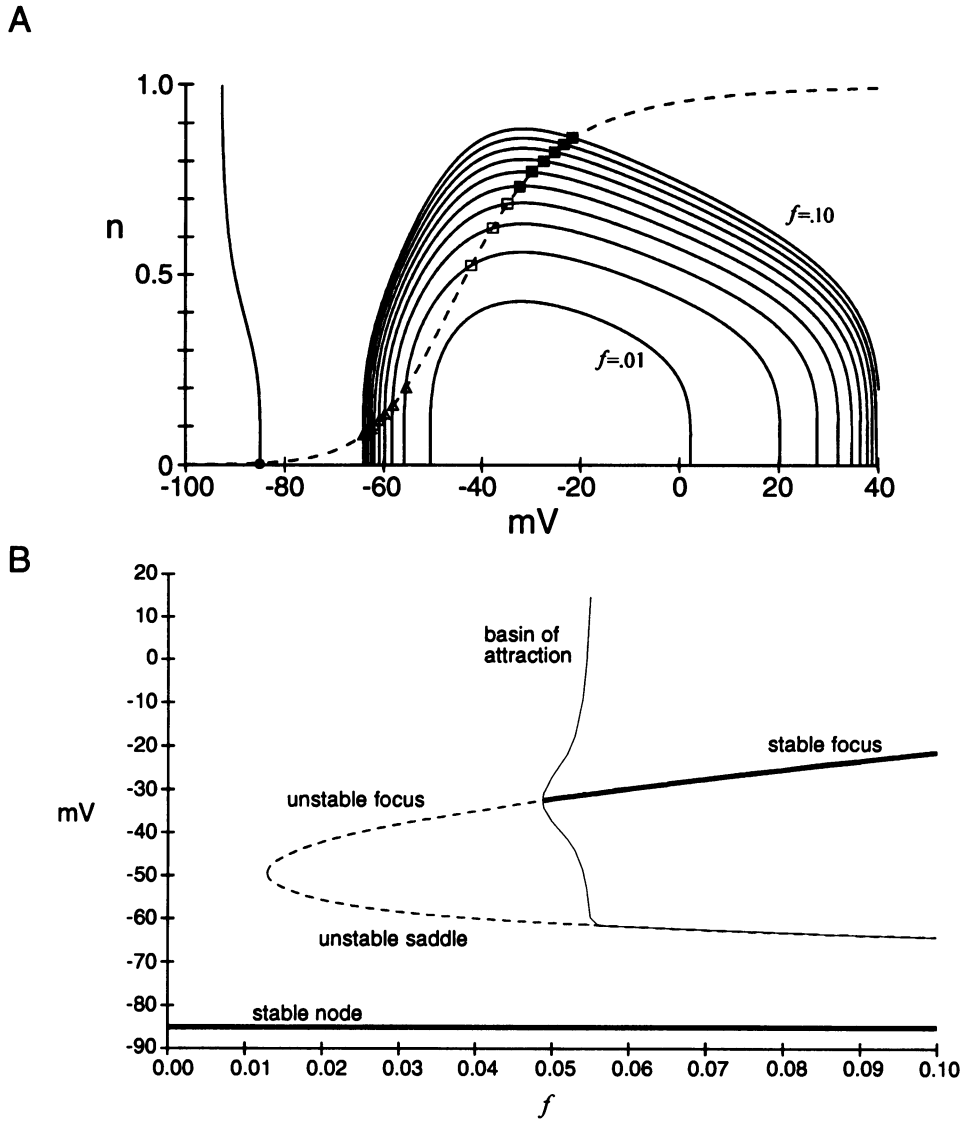

FIGURE 10 Phase portrait and bifurcation diagram for the reduced model with $[K]_o$ = 4 mM. (*A*) A family of nullclines is shown as f was varied from 0.01 to 0.10 in increments of 0.01. The n-nullcline (*dashed line*) is not dependent on f. Only the right-hand branch of the V-nullcline (*solid line*) is sensitive to changes in f. Equilibrium points occur where the n- and V-nullclines intersect. Stable equilibria are depicted with filled symbols: circles for nodes and squares for foci. Unstable equilibria are indicated by open symbols: triangles for saddles and squares for foci. Notice that a stable node occurs at a resting potential of −85 mV for all values of f. (*B*) The bifurcation diagram shows all possible equilibrium potentials at each value of f as it was varied from 0 to 0.1. The stability character of each equilibrium potential is indicated by the format of the line: solid lines for stable ones and broken lines for unstable. The pair of thin curves delineates the basin of attraction for the second stable equilibrium potential which appears when $f > 0.048$. At each value of f, the upper curve shows the most depolarized voltage contained within this basin, while the lower one indicates the most hyperpolarized potential in the basin. (See Fig. 11 for an example of a basin of attraction in the n-V plane.)

toward a stable focus as time progressed so that the time course was a damped oscillation. Unstable foci had complex-valued eigenvalues with real parts greater than 0. Local trajectories spiraled outward away from an unstable focus as time increased. This corresponded to unstable oscillations with progressively increasing amplitude in the time domain.

The information contained in a phase portrait (Fig. 10 *A*) can be summarized in a bifurcation diagram (Fig. 10 *B*). This diagram traces the loci of the equilibrium potentials as a parameter of the system is varied. In Fig. 10 *B* the equilibrium potentials are plotted with increasing f; $[K]_o$ is fixed at 4 mM. The stability of any equilibrium potential is indicated by the format of the line. The dynamical features implied by this bifurcation diagram have direct physiological correlates.

For the normal $[K]_o$ condition, a stable node always occurred at an equilibrium potential of −85 mV, over the entire interval of $0 \leq f \leq 0.1$. This means that the membrane voltage will always approach this resting potential monotonically, with no oscillations. This resting potential did not shift, because the left-hand branch of the V-nullcline is insensitive to changes in f (Fig. 10 *A*). As f increased, two additional equilibrium potentials were created. The three equilibria that occurred for any $f > 0.013$ are analogous to the multiple zero-current crossings of the full model depicted in the I_m-V

curves of Fig. 7. For values of $0.013 < f < 0.048$ the two new equilibrium potentials were both unstable. The dashed portion of the diagram traces the locus of the unstable focus created at the most depolarized equilibrium potential for a particular value of f. The surface potential will never come to rest at this value and create depolarization block of action potentials.

As f increased beyond 0.048, the depolarized equilibrium potential abruptly changed from an unstable focus to a stable one (transition from open to filled squares in Fig. 10 *A*). Therefore with these larger values of f, the membrane potential may settle to this new depolarized equilibrium position with an oscillatory time course. The existence of multiple stable equilibria divided the *n-V* phase plane into two regions; one where all trajectories settled monotonically at the more hyperpolarized stable node, the other where every trajectory spiraled into the depolarized stable focus. Each region is called a basin of attraction for a particular equilibrium potential. A competition between two stable equilibrium potentials is shown in Fig. 11, *A* and *B*. When the system started from the resting potential, then for every possible current pulse, the trajectory in the *n-V* plane returned to the original resting potential at −85 mV. This occurs because a brief current pulse always shifts the system horizontally in the *n-V* plane. As shown in Fig. 11 *A*, any horizontal deviation from the resting potential was outside the basin of attraction for the stable node at −31 mV (*shaded area*). If a depolarizing impulse is applied during the repolarizing phase of the action potential (*arrow*), however, then the system may jump to a second trajectory that lies within the basin of attraction for the stable focus (Fig. 11 *B*). The trajectory spirals toward the equilibrium potential, because the eigenvalues are complex at that singularity. The physiological implication is that all action potentials starting from the resting potential at −85 mV have a normal time course and return to the same membrane potential. If a current pulse is applied during the repolarizing phase of the action potential, however, then the membrane voltage may settle in a damped oscillatory fashion to the depolarized equilibrium potential. From this depolarized membrane voltage the system is incapable of producing a regenerative spike, because any depolarizing current pulse from this point in the *n-V* plane moves the system into a region where *dV/dt* is negative. It is analogous to depolarization block in a paralyzed fiber. However, the system can be returned to the normal resting potential by either a large depolarizing or hyperpolarizing input, so long as the input is sufficiently large to force the system to a trajectory in the basin of attraction for the resting potential at −85 mV (the *unshaded* region in Fig. 11 *A*). Finally there are no stable limit cycles in the bifurcation diagram in Fig. 10 *B*. This means that the system will never produce an infinite train of discharges. No matter what value f attains, the system always relaxes to one or the other stable equilibrium potential.

A change in $[K]_o$ leads to completely different forms of system behavior. The influence of $[K]_o$ can be visualized as changes in the shapes of the phase portrait and the bifurcation

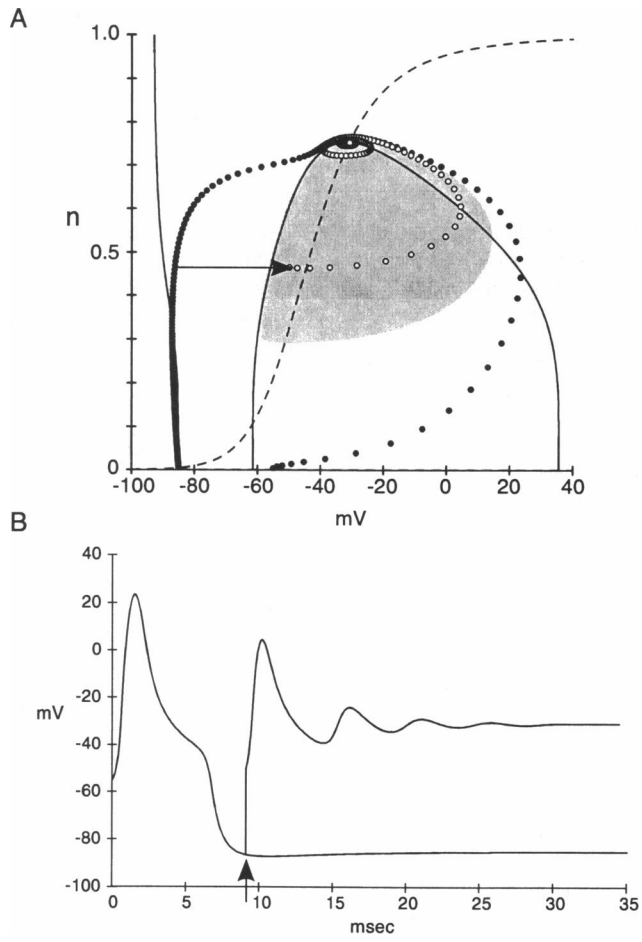

FIGURE 11 The reduced model can simulate a fiber with two possible equilibrium potentials. (*A*) Two separate trajectories are shown in the *n-V* phase plane. The shaded region shows the basin of attraction for the stable focus at −31 mV. The boundary for the basin of attraction to a stable focus was computed by starting at the equilibrium potential and integrating numerically backwards in time. All trajectories that enter this region will spiral toward the focus. The filled circles show the path that was traversed when the system was depolarized from a resting potential of −85 mV. Any current stimulus applied at the resting potential drives the system to a trajectory that lies outside the shaded region, and therefore the membrane potential returned to −85 mV. If a depolarizing current was applied during the repolarizing phase of an action potential before n recovered to < 0.3 (*arrow*), then the system was driven into the basin of attraction for the stable focus at −31 mV. The trajectory is plotted with a time increment of 0.1 ms; the integration time step was .01 ms. (*B*) The two action potentials corresponding to the trajectories in (*A*) are shown in the time domain. For this simulation, the reduced model was used with $f = 0.055$ and $[K]_o = 4$ mM.

diagram (Fig. 12). When $[K]_o$ equaled 10 mM, four major changes occurred. First, as f increased, the stable node that defined the resting potential did shift slightly in the depolarizing direction (Fig. 12 *B*). This implies that, unlike the case when $[K]_o = 4$ mM, an increase in the proportion of noninactivating sodium channels will cause a spontaneous, albeit small, depolarization of the resting potential. Second, beyond $f = 0.011$, this equilibrium potential no longer exists. The sudden change occurs because the *V*-nullcline shifts upward and loses the point of intersection with the *n*-nullcline as shown in Fig. 12 *A*. Also notice that with a higher $[K]_o$,

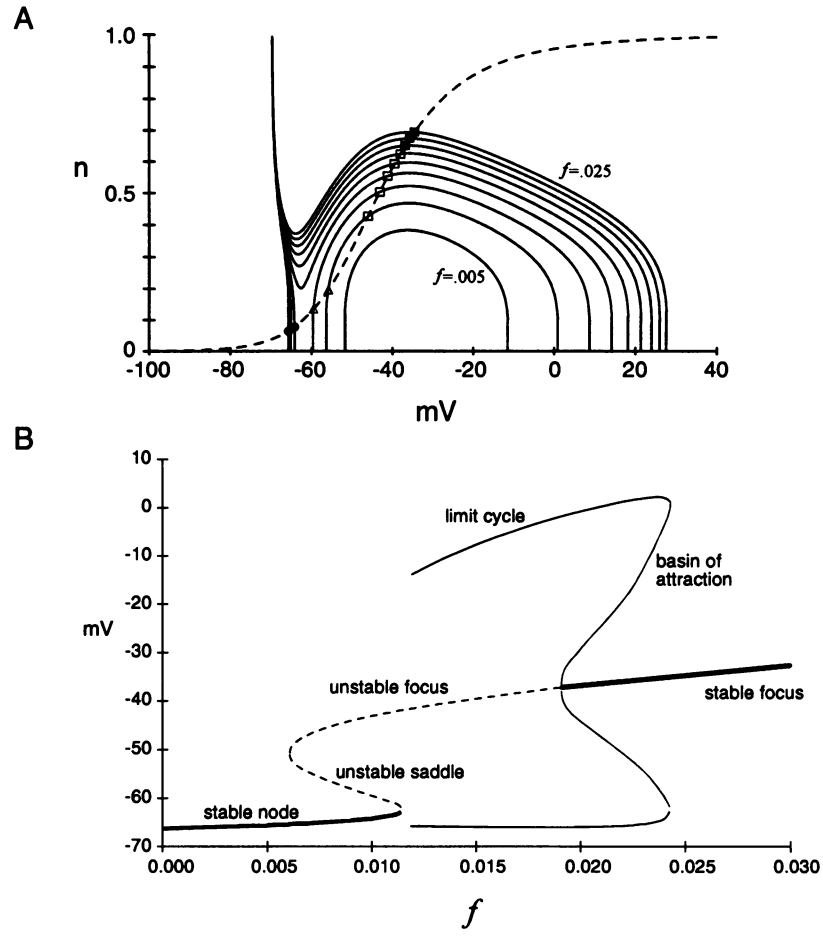

FIGURE 12 Phase portrait and bifurcation diagram for the reduced model with $[K]_o = 10$ mM. (*A*) A family of nullclines is shown as f was varied from 0.005 to 0.025 in increments of 0.0025. The resting potential at the stable node (*filled circles*) shifts in the depolarizing direction as f increases and then vanishes for $f > 0.011$. For each of the three nullclines where f was between 0.0125 and 0.0175, only one equilibrium potential occurred, and it was unstable (*open squares*). Under those conditions the membrane potential oscillated indefinitely in a limit cycle of constant amplitude. Symbols at each equilibrium potential (intersection of n- and V-nullclines) retain the same meaning as in Fig. 10. (*B*) The bifurcation diagram illustrates the value and stability character of each equilibrium potential as f is varied. The format of each curve indicates the stability for each of these singularities as in Fig. 10 *B*.

the first bifurcation (where new equilibrium potentials are created or destroyed) occurs at a lower value of f (0.012 vs. 0.0485). This is an example of the synergy between the depolarizing influence of raised extracellular K^+ and the destabilizing effect of the noninactivating sodium current, in producing an abnormal state of muscle excitability.

Moreover, in the interval where $0.011 < f < 0.019$ the single remaining equilibrium potential is unstable. This creates the third fundamentally different form of behavior. When there is no stable equilibrium potential, the system oscillates indefinitely as an infinitely long train of discharges with fixed amplitude as shown in Fig. 13 *B*. No form of current injection can drive the system toward a stable equilibrium. The only possible physiological state is myotonia. The trajectory of this oscillation traced a limit cycle on the n-V phase plane as shown in Fig. 13 *A*. Because the remaining equilibrium potential had complex-valued eigenvalues with positive real parts, trajectories near the equilibrium potential spiraled outward with time and asymptotically approached the limit cycle. Trajectories that began outside this loop spiraled inward with time to approach the limit cycle. The amplitude of the limit cycles increases with larger values of f as drawn in Fig. 12 *B*.

As f increased further, the equilibrium potential became stable for $f > 0.019$. Now two possible solutions exist; spiraling trajectories approaching the stable equilibrium potential or trajectories that spiral inward or outward toward the limit cycle. A trajectory that spiraled in toward this limit cycle is shown in Fig. 13 *C*. During the repolarizing phase, a depolarizing impulse of current was applied (*arrow*). This jumped V to a trajectory inside the limit cycle, within the basin of attraction of the stable focus, and the path spiraled inward toward the equilibrium potential. A similar escape from the limit cycle occurred if a hyperpolarizing current pulse was applied near the peak of the action potential. Physiologically two possible states occurred with this type of phase portrait: an infinite train of myotonic discharges with fixed amplitude or a damped oscillation in V that eventually settled to the equilibrium potential. As f increased, the basin of attraction for the stable focus increased; that is, trajectories in a larger and larger region of the phase plane spiraled toward this equilibrium potential.

Eventually at $f = 0.0245$ the fourth major change in system behavior occurred. The basin of attraction for the stable focus expanded to encompass the entire plane, and the limit cycle was lost as a possible solution. The system always came to rest at this depolarized equilibrium potential. From this equilibrium position, the system is incapable of producing a regenerative depolarization in response to a depolarizing current stimulus. This state is analogous to the block of action potential generation that occurs in a depolarized segment of a muscle fiber. Recall that a depolarizing current pulse moves V directly horizontally and to the right in the n-V plane. With these large values of f, the V nullcline had a negative slope

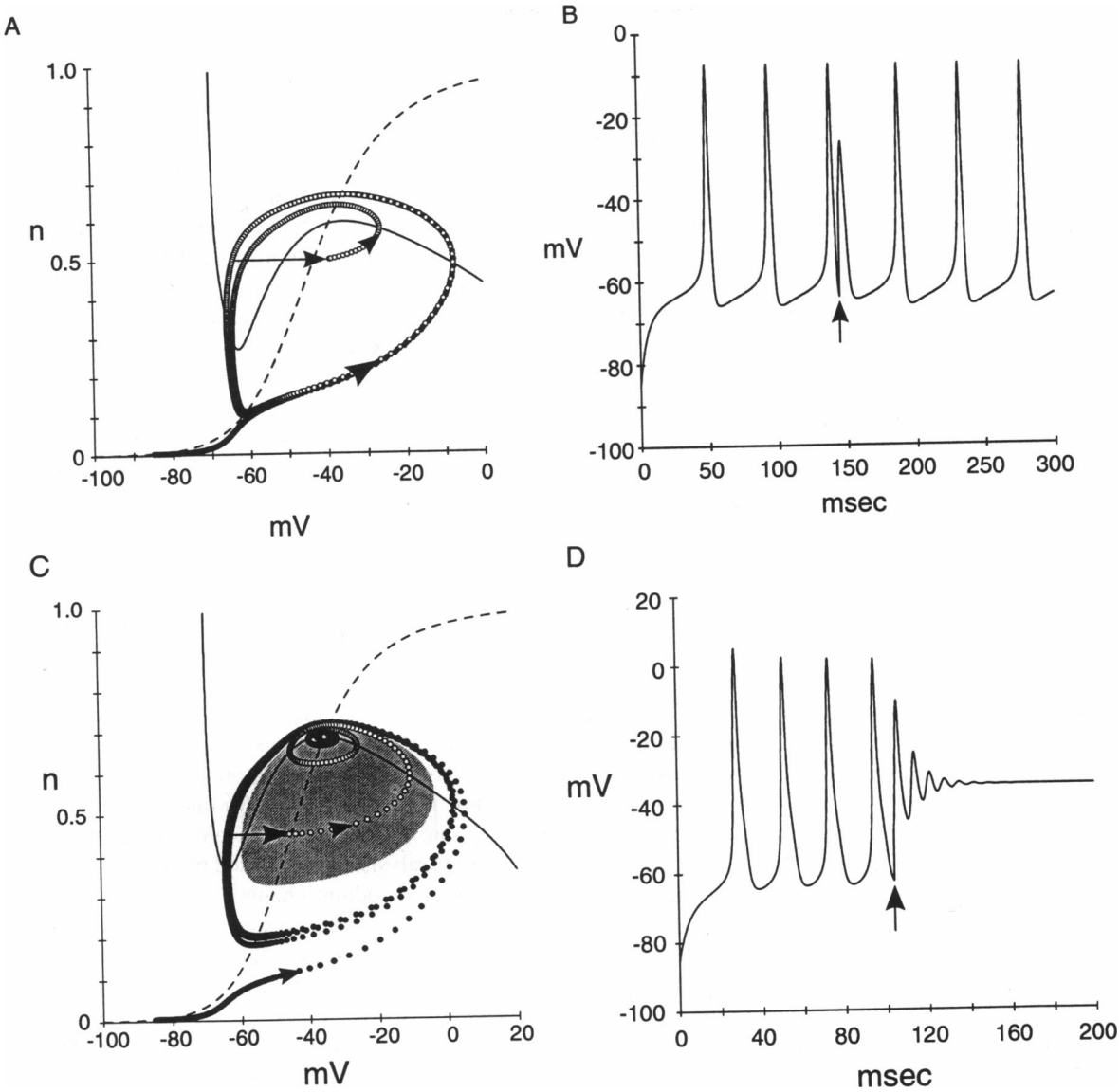

FIGURE 13 Two examples of limit cycle behavior for the reduced model. (*A*) The trajectory in the *n-V* phase plane depolarizes spontaneously from an arbitrarily set initial membrane potential of −85 mV (*filled circles*). After three repetitive discharges, the membrane was depolarized by 20 mV (*thin arrow*). This input caused the system to jump to a trajectory (*open circles*) that started in the vicinity of the unstable equilibrium potential. Oscillations in the membrane voltage occurred with increasing amplitude until the trajectory spiraled out to the same limit cycle. With $f = 0.015$ and $[K]_o = 10$ mM all trajectories terminated on this limit cycle. (*B*) The membrane voltage is shown in the time domain for the same simulation as in *A*. In *C* and *D*, *f* was increased to 0.024. With a larger proportion of noninactivation Na^+ channels, the equilibrium potential converted to a stable focus with an associated basin of attraction (*shaded* region). All trajectories starting outside the limit cycle spiraled in toward it. From the interior of the limit cycle, trajectories either spiraled outward or inward toward the stable focus, depending on whether they were inside or outside of the basin of attraction, respectively. (*D*) The time course is shown for a trajectory that started outside the limit cycle. A depolarizing current pulse at the end of an action potential drove the system to an adjacent trajectory that was inside the basin of attraction for the stable focus.

at the equilibrium potential in the *n-V* plane as shown in Fig. 12 *A*. Therefore, any depolarizing pulse always displaced *V* into a region where $dV/dt < 0$ and the membrane repolarized. In addition, since dn/dt is positive at all regions to the right of the *n* nullcline the trajectory can never pass downward into a region where $dV/dt > 0$. There is never any possibility of a regenerative current to further depolarize the membrane. At these depolarized equilibrium potentials, the outward potassium current always exceeds the inward Na^+ current, because *n* started out with a large value. If a hyperpolarizing current pulse is applied from this equilibrium potential, then a regenerative response will occur with a transient that overshoots the equilibrium potential in the depolarizing direction. This simulation is analogous to anodal break that elicits an action potential when a hyperpolarizing current injection is removed.

DISCUSSION

A model has been presented to explore the mechanism by which a loss of sodium channel inactivation may dramatically alter the electrical response of a muscle fiber. Several

inherited disorders of muscle excitability have been attributed to a disruption of inactivation for sodium channels. In patch-clamp recordings from affected muscle, however, the fraction of channels that fails to inactivate is small: on the order of a few percent (6, 14, 15). Therefore, it is important to establish that even a small proportion of noninactivating sodium channels is sufficient to produce the myotonia and paralysis that occur in these disorders. One approach is to induce a partial loss of sodium channel inactivation in normal muscle and then observe any changes in behavior. We have used a toxin from the anemone (ATX II) to demonstrate that failure of inactivation in as little as 2% of the sodium channels is sufficient to cause myotonia (17). The quantitative model presented herein complements these experimental observations by allowing a more precise control of the sodium channel defect and by providing insight into the relative importance of the many factors that impinge upon the behavior of the whole fiber.

Although the model incorporates many simplifying assumptions, it simulates a rich variety of responses which can be correlated to phenomena observed in muscle. Perhaps the most robust conclusion is that a loss of inactivation in a small proportion of sodium channels is sufficient to cause a second possible steady-state for the membrane potential. When 5% of the sodium channels fail to inactivate, a new equilibrium potential is created that is depolarized by about 50 mV from the normal resting potential (see Fig. 10 *B*). If the extracellular K^+ is elevated, then as little as 2% of noninactivating channels can create a 30-mV shift in the equilibrium potential (cf. Fig. 12 *B*). These large shifts occur because the $\bar{g}_{Na}$ is approximately six times larger than $\bar{g}_K$ (see Table 1). Consequently, a large membrane depolarization is required to open a large enough fraction of K^+ channels to balance the current passed by even a small proportion of noninactivating Na^+ channels. This is further supported by the observation that increasing the effective $\bar{g}_K$ with Cromakalim and related K^+ channel openers hyperpolarizes the membrane and alleviates the weakness in hyperkalemic periodic paralysis (36).

An impairment of sodium channel inactivation does contribute to the development of myotonia, but additional factors are required to sustain the train of action potentials. Both the toxin experiments on rat muscle (17) and the model simulations demonstrate that the electrical integrity of the T-tubule system is necessary to produce sustained runs of myotonic discharges. This is a feature in common between the myotonia produced by a low chloride conductance in the goat (21) and that produced by the defective sodium channel in HPP and paramyotonia congenita. As first proposed by Adrian and Bryant, it is probably an accumulation of K^+ in the lumen of the T-tubule that drives the train of discharges after the end of a current pulse (21). In fact, the inability of an earlier version of the model to generate sustained runs of action potentials led us to add a second, "T-tubule" compartment to our model. With a model, the "thought experiment" can be performed wherein K^+ accumulation is prevented without otherwise changing the capacitive load or ionic conductance of the T-tubule. This cannot be achieved experimentally, but in agreement with the simulations of Adrian and Marshall (20), we conclude that the K^+ accumulation is the critical feature of the T-tubule compartment that promotes repetitive firing.

The reduced version of our model simulates an isolated patch of membrane and can be represented conveniently in the *n-V* phase plane. It shows explicitly that the combination of a noninactivating sodium current and an elevated extracellular K^+ not only enables myotonia to occur, but also may lead to a state in which the only possible long-term behavior is repetitive firing with no stable equilibrium potential (Figs. 12 *B*, 13 *A*, and 13 *B*). This illustrates that the local K^+ gradient, and not some distributed network property of the T-tubule, drives the train of spikes. Of course, in a physiological preparation the sustained firing would alter the extracellular K^+ so that the cell would not discharge indefinitely. Rather, the progressive increase in K^+ would cause the membrane potential to settle on a depolarized value (cf. Fig. 5 *C*). Conversely, when the extracellular K^+ is normal or low (see Fig. 10 *B*) then the system can not produce an infinite train of discharges. At least one stable equilibrium potential always exists over the entire range of *f*, and there are no limit cycles. Perhaps this absence of limit cycles in the phase diagram for low values of K^+ is an explanation for the extreme rarity of having myotonia in an individual with *hypo*kalemic periodic paralysis. In that disorder, the muscle is also depolarized to about −55 mV during attacks of weakness, and paralysis is also caused by depolarization-induced inactivation of sodium channels. Unlike the hyperkalemic case, however, during episodes of hypokalemic periodic paralysis the extracellular K^+ is 2–3.5 mM which might prevent the membrane from sustaining a repetitive train of discharges.

The model demonstrates that a [K]-dependent development of myotonia or paralysis in muscle with disrupted Na^+ channel inactivation does not necessarily imply that the defect in Na^+ channel function is [K] dependent. The consequence of a sodium conductance that does not completely inactivate depends strongly upon the ratio of $[K]_o/[K]_i$ as shown in Figs. 5, 10 *B*, and 12 *B*. The recognition of this interdependence between *f* and $[K]_o$ is important when considering the mechanism by which Na^+ channel defect(s) may cause myotonia or paralysis. In human muscle fibers cultured from one family with hyperkalemic periodic paralysis (HPP), the probability of a Na^+ channel gating in the noninactivating mode increased with higher extracellular [K] (6). This provided a satisfying explanation for the episodic nature of the disease: myotonia or paralysis occur only when the serum [K] is elevated and alters the channel gating. Across different families with HPP or paramyotonia congenita (PC), however, many different point mutations have been identified in the a subunit of the skeletal muscle Na^+ channel (reviewed in Ref. 37). It is highly unlikely that all of these mutations cause an extracellular [K]-dependent loss of inactivation. Yet, in voltage-clamp measurements on fibers from many affected families, in either high or sometimes normal [K], there was

a noninactivating, TTX-sensitive Na^+ current (2, 3). It is now known that the families who participated in these voltage-clamp studies have different mutations of the α subunit (F. Lehmann-Horn, personal communication). The different point mutations of the α subunit may all disrupt inactivation, but they might not all be K^+-dependent. Several mutations are located on the cytoplasmic end of putative transmembrane segments that lie adjacent to the pore-forming region of the S5–S6 loop and could thereby influence the binding of an inactivation particle to the inner vestibule of the pore. The simulations of our model demonstrate that a small (fixed) proportion of noninactivating sodium channels may either have no effect, cause myotonia, or cause paralysis due to a large depolarizing shift in the resting potential, and that this variety of responses can occur by varying only the extracellular [K]. Thus it is not necessarily valid to conclude that a point mutation of the α subunit, identified in a family with a K^+-dependent phenotype of paralysis or myotonia, causes a K^+-dependent alteration in Na^+ channel function. Such mechanistic questions must be addressed by either recording Na^+ channel gating in patches from biopsied fibers or by functional expression and characterization of mutant channels.

APPENDIX: STABILITY ANALYSIS OF THE REDUCED MODEL

The reduced model defined by Eqs. 23 and 24 was analyzed by finding equilibrium positions of the system and determining the stability of each equilibrium. Equilibria occur at critical points, $(\hat{n},\hat{V})$, where $dV/dt = 0$ and $dn/dt = 0$ simultaneously. These loci were determined numerically by iteratively varying V in Eq. 23 until dV/dt was arbitrarily close to 0. In this computation $n(V,t)$ was set equal to $n_\infty(V)$ so that Eq. 24 would be satisfied simultaneously. An equilibrium point is stable if any nearby point $(\hat{n}+\delta, \hat{V}+\delta)$ remains nearby for all future time. If the system tends toward $(\hat{n},\hat{V})$ as t approaches infinity, then the equilibrium is asymptotically stable. The stability of any equilibrium point in a nonlinear system is identical to the stability of a first-order approximation of the system at that point. Using this fact, the problem is reduced to an analysis of the stability of a linear system which is easily computed from the roots of the characteristic equation (eigenvalues). For Eqs. 23 and 24 the linearized system in the neighborhood of an equilibrium point is:

$$\begin{Bmatrix} \dot{V} \\ \dot{n} \end{Bmatrix} = \begin{bmatrix} F_{1,V} & F_{1,n} \\ F_{2,V} & F_{2,n} \end{bmatrix} \begin{Bmatrix} V \\ n \end{Bmatrix} \tag{A1}$$

where $F_1(V,n)$ is the right-hand side of Eq. 23, $F_2(V,n)$ is the right-hand side of Eq. 24, and $F_{i,j} = \partial F_i/\partial_j$ evaluated at the equilibrium point $(\hat{n},\hat{V})$. The partial derivatives can be computed in closed form from Eqs. 10–12, 23, 24, but it was easier to compute them numerically as

$$F_{i,j} = \frac{F_i(j+\epsilon) - F_i(j)}{\epsilon} \tag{A2}$$

where $\epsilon = 0.00001 \times j$. Finally, the eigenvalues, λ, were computed as the roots of the characteristic equation for the Jacobian matrix in Eq. A1,

$$\lambda^2 + (F_{1,V} + F_{2,n})\lambda + F_{1,n}F_{2,V} - F_{1,V}F_{2,n} = 0. \tag{A3}$$

As time proceeds, n and V change in proportion to $e^{\lambda t}$ and hence the sign of the real part of λ determines the stability as detailed under Results.

This work was supported by the National Institutes of Health (grant R01 AR41025-1), a fellowship from the Charles A. Dana Foundation (to S. C. Cannon), and by the Howard Hughes Medical Institute (to S. C. Cannon and D. P. Corey). R. H. Brown was supported by the Cecil B. Day Foundation and the Muscular Dystrophy Association.

REFERENCES

1. Rüdel, R., and F. Lehmann-Horn. 1985. Membrane changes in cells from myotonia patients. *Physiol. Rev.* 65:310–356.
2. Lehmann-Horn, F., R. Rüdel, K. Ricker, H. Lorkovic, R. Dengler, and H. C. Hopf. 1983. Two cases of adynamia episodica hereditaria: in vitro investigation of muscle cell membrane and contractile parameters. *Muscle and Nerve.* 6:113–121.
3. Lehmann-Horn, F., G. Küther, K. Ricker, P. Grafe, K. Ballanyi, and R. Rüdel. 1987. Adynamia episodica hereditaria with myotonia: a noninactivating sodium current and the effect of extracellular pH. *Muscle and Nerve.* 10:363–374.
4. Ricker, K., L. M. Camacho, P. Grafe, F. Lehmann-Horn, and R. Rüdel. 1989. Adynamia episodica hereditaria: what causes the weakness? *Muscle and Nerve.* 12:883–891.
5. Lehmann-Horn, F., R. Rüdel, R. Dengler, H. Lorkovic, A. Haass, and K. Ricker. 1981. Membrane defects in paramyotonia congenita with and without myotonia in a warm environment. *Muscle and Nerve.* 4:396–406.
6. Cannon, S. C., R. H. Brown, and D. P. Corey. 1991. A sodium channel defect in hyperkalemic periodic paralysis: potassium-induced failure of inactivation. *Neuron.* 6:619–626.
7. Fontaine, B., T. S. Khurana, E. P. Hoffman, G. A. P. Bruns, J. L. Haines, J. A. Trofatter, M. P. Hanson, J. Rich, H. McFarlane, Y. D. McKenna, D. Romano, J. F. Gusella, and R. H. Brown, Jr. 1990. Hyperkalemic periodic paralysis and the adult muscle sodium channel α-subunit gene. *Science.* 250:1000–1002.
8. Ebers, G. C., A. L. George, R. L. Barchi, S. S. Ting-Passador, R. G. Kallen, G. M. Lathrop, J. S. Beckmann, A. F. Hahn, W. F. Brown, R. D. Campbell, and A. J. Hudson. 1991. Paramyotonia congenita and hyperkalemic periodic paralysis are linked to the adult muscle sodium channel gene. *Ann. Neurol.* 30:810–816.
9. Ptacek, L. J., J. S. Trimmer, W. S. Agnew, J. W. Roberts, J. H. Petajan, and M. Leppert. 1991. Paramyotonia congenita and hyperkalemic periodic paralysis map to the same sodium-channel gene locus. *Am. J. Human Genet.* 49:851–854.
10. Rojas, C. V., J. Wang, L. S. Schwartz, E. P. Hoffman, B. R. Powell, and R. H. Brown. 1991. A Met-to-Val mutation in the skeletal muscle Na channel α-subunit in hyperkalemic periodic paralysis. *Nature.* 354:387–389.
11. Ptacek, L. J., A. L. George, R. C. Griggs, R. Tawil, R. G. Kallen, R. L. Barchi, M. Robertson, and M. F. Leppert. 1991. Identification of a mutation in the gene causing hyperkalemic periodic paralysis. *Cell.* 67:1021–1027.
12. McClatchey, A. I., P. Van den Bergh, M. A. Pericak-Vance, W. Raskind, C. Verellen, D. McKenna-Yasek, K. Rao, J. L. Haines, T. Bird, R. H. Brown, and J. F. Gusella. 1992. Temperature-sensitive mutations in the III–IV cytoplasmic loop region of the skeletal muscle sodium channel gene in paramyotonia congenita. *Cell.* 68:769–774.
13. Cannon, S. C., and S. M. Strittmatter. 1993. Functional expression of sodium channel mutations identified in families with periodic paralysis. *Neuron.* 10:317–326.
14. Franke, C., H. Hatt, P. A. Iazzo, F. Lehmann-Horn. 1990. Characteristics of Na channels and Cl conductance in resealed muscle fibre segments from patients with myotonic dystrophy. *J. Physiol.* 425:391–405.
15. Franke, C., P. A. Iazzo, H. Hatt, W. Spittlemeister, K. Ricker, and F. Lehmann-Horn. 1991. Altered Na channel activity and reduced Cl conductance cause hyperexcitability in recessive generalized myotonia (Becker). *Muscle and Nerve.* 14:762–770.
16. Lehmann-Horn, F., P. A. Iazzo, C. Franke, H. Hatt, and F. Spaans. 1990. Schwartz-Jampel syndrome: II Na channel defect causes myotonia. *Muscle and Nerve.* 13:528–535.
17. Cannon, S. C., and D. P. Corey. 1993. Loss of sodium channel inactivation by anemone toxin (ATX II) mimics the myotonic state in hyperkalemic periodic paralysis. *J. Physiol.* 466:501–520.
18. Steinberg, I. Z. 1988. Computer simulations of the effect of noninactivating sodium channels on the electric behavior of excitable cells. *J. Theoret. Biol.* 133:193–214.

19. Steinberg, I. Z. 1990. Computer simulations of electrical bistability in excitable cells due to non-inactivating sodium channels: space- and time-dependent behavior. *J. Theoret. Biol.* 144:75–92.
20. Adrian, R. H., and M. W. Marshall. 1976. Action potentials reconstructed in normal and myotonic muscle fibres. *J. Physiol.* 258:125–143.
21. Adrian, R. H., and S. H. Bryant. 1974. On the repetitive discharge in myotonic muscle fibres. *J. Physiol.* 240:505–515.
22. Adrian R. H., and L. D. Peachy. 1973. Reconstruction of the action potential in frog sartorius muscle. *J. Physiol.* 235:103–131.
23. Adrian, R. H., L. L. Constantin, and L. D. Peachy. 1969. Radial spread of contraction in frog muscle fibres. *J. Physiol.* 204:231–257.
24. Peachy, L. D. 1965. The sarcoplasmic reticulum and transverse tubules of the frog's sartorius muscle. *J. Cell. Biol.* 25:209–231.
25. Palade, P. T., and R. L. Barchi. 1977. Characteristics of the chloride conductance in muscle fibers of the rat diaphragm. *J. Gen. Physiol.* 69:325–342.
26. Almers, W. 1972. Potassium conductance changes in skeletal muscle and the potassium concentration in the transverse tubules. *J. Physiol.* 225:33–56.
27. Freygang, W. H., D. A. Goldstein, and D. C. Hellam. 1964. The after-potential that follows trains of impulses in frog muscle fibers. *J. Gen. Physiol.* 47:929–952.
28. Adrian, R. H., and M. W. Marshall. 1977. Sodium currents in mammalian muscle. *J. Physiol.* 268:223–250.
29. Pappone, P. A. 1980. Voltage-clamp experiments in normal and denervated mammalian skeletal muscle fibres. *J. Physiol.* 306:377–410.
30. Beam, K. G., and P. L. Donaldson. 1983. A quantitative study of potassium channel kinetics in rat skeletal muscle from 1 to 37°C. *J. Gen. Physiol.* 81:485–512.
31. Almers, W., W. M. Roberts., and R. L. Ruff. 1984. Voltage clamp of rat and human skeletal muscle: measurements with an improved loose-patch technique. *J. Physiol.* 347:751–768.
32. Jaimovich, E., R. A. Venosa, P. Shrager, and P. Horowicz. 1976. Density and distribution of tetrodotoxin receptors in normal and detubulated frog sartorius muscle. *J. Gen. Physiol.*. 67:399–416.
33. Caillé, J., M. Ildefonse, and O. Rougier. 1978. Existence of a sodium current in the tubular membrane of frog twitch muscle fibre: its possible role in the activation of contraction. *Pflügers Arch.* 374:167–177.
34. Eisenberg, R. S., and P. W. Gage. 1969. Ionic conductances of the surface and transverse tubular membranes of frog sartorius fibers. *J. Gen. Physiol.* 53:279–297.
35. Thompson, J. M. T., and H. B. Stewart. 1988. Nonlinear Dynamics and Chaos. John Wiley and Sons, New York. 375 pp.
36. Quasthoff, S., M. Strupp, A. Spuler, F. Lehmann-Horn, and P. Grafe. 1990. Enhancement of K^+ conductance improves in vitro the contraction force of skeletal muscle from patients with periodic paralysis. *Pflügers Arch.* 415:R117.
37. Caldwell, J. H., and K. Schaller. 1992. Opening the gates on ion channel diseases. *Nature Genet.* 2:87–89.